Cell Reports

Resource

Inflammaging is driven by upregulation of innate immune receptors and systemic interferon signaling and is ameliorated by dietary restriction

Graphical abstract

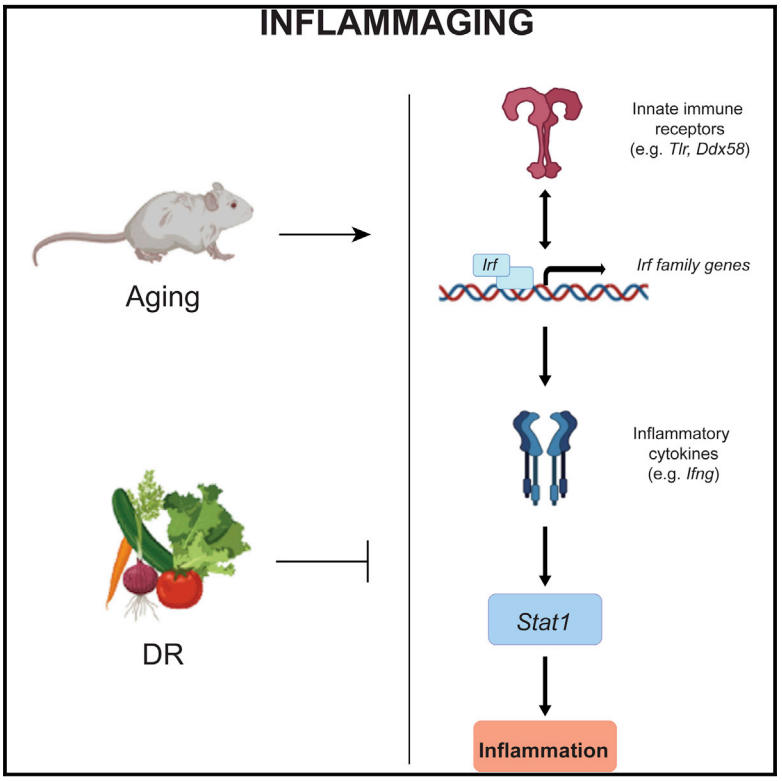

Authors

Seyed Mohammad Mahdi Rasa, Francesco Annunziata, Anna Krepelova, ..., Karl Lenhard Rudolph, Alessandro Ori, Francesco Neri

Correspondence

francesco.neri@unito.it

In brief

Using transcriptomic analysis and chromatin accessibility assays, Rasa et al. identify the multi-tissue gene network regulating inflammaging. These effects can be partially reversed via dietary intervention in a tissue-specific manner.

Highlights

- Innate immune system receptors/interferon/Stat1 axis triggers inflammaging
- Both lifetime and short-time dietary restriction (DR) treatments ameliorate inflammaging
- Transcriptome alteration caused by aging, lifetime, or short-term DR are tissue specific
- Aging induces a general open chromatin rearrangement, which is not rescued by DR

Rasa et al., 2022, Cell Reports *39*, 111017
June 28, 2022
https://doi.org/10.1016/j.celrep.2022.111017

CellPress

Cell Reports

CellPress
OPEN ACCESS

Resource

Inflammaging is driven by upregulation of innate immune receptors and systemic interferon signaling and is ameliorated by dietary restriction

Seyed Mohammad Mahdi Rasa,[1,4] Francesco Annunziata,[1,4] Anna Krepelova,[1,3] Suneetha Nunna,[1] Omid Omrani,[1] Nadja Gebert,[1] Lisa Adam,[1] Sandra Käppel,[1] Sven Höhn,[2] Giacomo Donati,[3] Tomasz Piotr Jurkowski,[2] Karl Lenhard Rudolph,[1] Alessandro Ori,[1] and Francesco Neri[1,3,5,*]

[1]Leibniz Institute on Aging – Fritz Lipmann Institute (FLI), Jena, Germany
[2]School of Bioscience, Cardiff University, Cardiff CF10 3AX, UK
[3]Department of Life Sciences and Systems Biology, University of Torino, Torino, Italy
[4]These authors contributed equally
[5]Lead contact
*Correspondence: francesco.neri@unito.it
https://doi.org/10.1016/j.celrep.2022.111017

SUMMARY

Aging is characterized by a chronic low-grade inflammation known as inflammaging in multiple tissues, representing a risk factor for age-related diseases. Dietary restriction (DR) is the best-known non-invasive method to ameliorate aging in many organisms. However, the molecular mechanism and the signaling pathways that drive inflammaging across different tissues and how they are modulated by DR are not yet understood. Here we identify a multi-tissue gene network regulating inflammaging. This network is characterized by chromatin opening and upregulation in the transcription of innate immune system receptors and by activation of interferon signaling through interferon regulatory factors, inflammatory cytokines, and Stat1-mediated transcription. DR ameliorates aging-induced alterations of chromatin accessibility and RNA transcription of the inflammaging gene network while failing to rescue those alterations on the rest of the genome. Our results present a comprehensive understanding of the molecular network regulating inflammation in aging and DR and provide anti-inflammaging therapeutic targets.

INTRODUCTION

In the last decades, as the average human lifespan has increased, the study of aging and aging-related diseases has acquired particular importance for our society. Aging can be defined by several hallmarks: mitochondrial dysfunction, epigenetic alteration, genomic instability, telomere attrition, loss of proteostasis, deregulated nutrient sensing, cellular senescence, stem cell exhaustion, and altered intercellular communication (Lopez-Otin et al., 2013). This leads to a gradual decrease of physiological organ function, higher risk of disease and, ultimately, death (Aunan et al., 2016). A prominent aging-associated condition is a chronic inflammation referred to as "inflammaging," a pro-inflammatory phenotype that accompanies aging in mammals (Salminen et al., 2012). Inflammaging is a highly significant risk factor for most, if not all, aging-related diseases including obesity and type 2 diabetes, cardiovascular diseases, Alzheimer's disease, and cancer, as well as vulnerability to infectious disease and vaccine failure (Barzilai et al., 2012; Baylis et al., 2013; Franceschi et al., 2017).

Dietary restriction (DR) decreases the calorie intake without inducing malnutrition. Lifetime DR is a non-pharmacological intervention that can extend the lifespan in a wide range of organisms, from yeast to worms, flies, rodents, and monkeys (Colman et al., 2009). Also, in humans DR improves health parameters (Fontana et al., 2010). Different mechanisms have been proposed to explain the beneficial effects of DR including reduction of body fat, attenuation of hormonal changes, increase in repair and damage removal pathways including autophagy and apoptosis, reduction in growth-promoting pathways such as *IGF1*/insulin and *mTOR*, and activation of health-promoting stress responses such as Sirtuin signaling (Kazemi et al., 2020). It has been shown that long-term DR (LTDR) also reduces some aspects of inflammation, leading to the hypothesis that a life-long energy accumulation can be the origin of chronic inflammation (Ye and Keller, 2010; Meydani et al., 2016). A very recent study carried out in rats has shown that late-life DR attenuated aging-related changes in cell type composition and gene expression, and reversed the aging-associated increase of senescence markers and alterations of the immune system (Ma et al., 2020). However, it is still largely unknown which signaling pathways and networks regulate the induction of inflammaging across tissues and whether DR could have an impact on rescuing such systemic induction of inflammaging.

Moreover, despite the aforementioned beneficial effects of DR, a long-term DR regimen has been shown to also have side

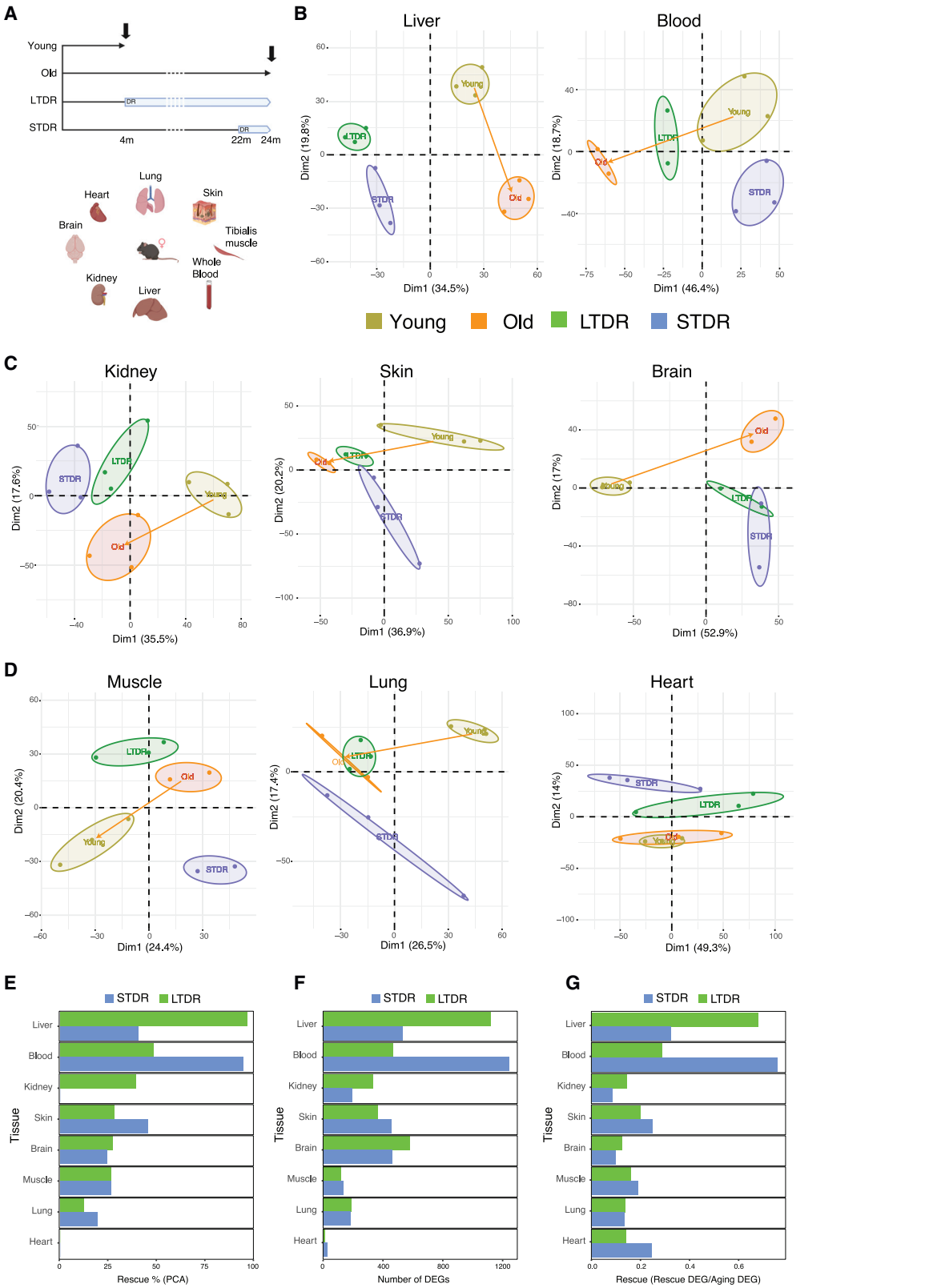

(legend on next page)

effects: changes in physical appearance, increased sensitivity to the cold, reduced muscle strength, menstrual irregularities, infertility, loss of libido, osteoporosis, slower wound healing, food obsession, irritability, and depression (Arends et al., 2017; Das et al., 2017; Dirks and Leeuwenburgh, 2006; Fontana and Partridge, 2015). To this end, alternative approaches have been sought, preserving the positive characteristics of DR while avoiding its drawbacks, such as short-term DR (STDR) treatments, repeated induction of short-term starvation/DR treatments, time-restricted feeding (Longo and Panda, 2016), intermittent fasting (IF) (Liu et al., 2020), and fast mimicking diets (Nencioni et al., 2018). Moreover, there is evidence that the capacity of DR to induce health benefits is lost at an advanced age. When DR is applied at a late age, reduction in mortality rates compared with *ad libitum* (AL) fed mice was greatly reduced compared with young-age interventions, and, moreover, transcriptional and metabolic response seemed to be attenuated in some tissues (Hahn et al., 2019).

In this study we employ a transcriptome-wide and multi-tissue approach to analyze the influence of both LTDR and STDR at old age on the aging phenotype. We were able to characterize a common transcriptional gene network driving inflammaging in most of the analyzed tissues. We also found that both DR interventions ameliorate this inflammaging phenotype, albeit with some differences mainly at tissue-specific level. Further chromatin accessibility analysis showed that DR can also rescue the aging-associated epigenetic alteration on the inflammaging-related genes, but not the genome-wide impairment of chromatin that accompanies old cells.

RESULTS

Aging-induced transcriptional changes are partially rescued by DR in most tissues

To understand the molecular mechanism of aging and DR, we performed transcriptional profiling using RNA sequencing (RNA-seq) of eight different tissues (blood, brain, heart, kidney, liver, lung, muscle, and skin) upon aging and DR. Animals were either kept on following four dietary regiments: AL fed young mice (4 months), AL fed old mice (24 months), long-term dietary restricted (LTDR; mice kept in DR from an age of 4 to 24 months), and short-term dietary restricted (STDR; old mice kept for 22 months on AL diet followed by 2 months in DR before sacrifice) (Figures 1A and S1A).

To have a multi-tissue overview and systematically compare different tissues, we performed, for each tissue, the principal component analysis (PCA) that can capture the linear correlation between the samples as well as relative distance and direction between the groups (Figures 1B–1D). All of the tissues, except heart, showed an age-dependent separation of the samples (orange line) indicating that aging does actually impact on the transcriptome of each tissue. By projecting the DR sample clusters on the aging axis (orange line), we could infer the percentage of DR-mediated rescue of the aging-associated transcriptional phenotype (scheme in Figure S1B). Interestingly, all tissues (except heart, which did not show clear, aging-related transcriptome changes) showed a rescue of this aging-associated phenotype following DR treatments, with LTDR being the most effective on liver and the STDR on blood (Figure 1E). The distances between DR clusters and the aging axis indicate instead a DR-mediated transcriptional response in the specific tissues on genes that are not altered in aging.

Moreover, we calculated the number of the differentially expressed genes (DEGs) (Table S1) (adjusted p value <0.05) (Figure S1C). Even though the number of statistically significant DEGs can be affected by the number of replicates and the intra-group variability, the observed differences among the different tissues indicated that some tissues (e.g., liver, blood, and kidney as expected) have a stronger transcriptional response following DR, while other tissues are lowly affected by DR or age (e.g., heart) (Figure S1C). Despite small differences, the number of DEGs that show the opposite regulation in respect to aging (Figures 1F and 1G) confirmed the results of the PCA data, strongly supporting the evidence that, in most of the analyzed tissues, DR can, to different extents, revert the aging phenotype at transcriptional level. Analysis of the rescued genes related to each of the functional categories in aging confirmed the PCA analysis, with blood being the most rescued in STDR and the liver in LTDR (Figures S1D and S1E).

Molecular pathways altered by aging and ameliorated by LTDR and/or STDR treatments

Using the DEGs, we defined significantly enriched canonical pathways in each tissue in aging and DR. Molecular pathways related to inflammation, metabolic pathways, and signaling pathways were the most enriched categories in aging and DR in different tissues (Figure 2A). However, the effects of aging, LTDR, and STDR were tissue specific. The difference between tissues mainly reflected the function of each tissue and/or its response to DR. For instance, upon DR (both LTDR and STDR) inflammation-related pathways were the most enriched category in the blood, which is largely composed of cells of the immune

Figure 1. DR partially rescues aging transcriptome

(A) Scheme of the experimental setting and of the harvested tissues.

(B–D) The principal component analysis (PCA) plot for each of the eight tissues (liver, blood [B], kidney, skin, brain [C], muscle, lung, and heart [D]) and four conditions (young, old, LTDR, and STDR) calculated on the basis of RNA-seq data. Orange line represents the minimal distance between young and old sample clusters. The tissues are ordered based on the percentage of rescue for LTDR (from bigger to smaller, E). The same order has been kept for the other plots. For each condition we used $\geq$4 mice.

(E) Rescue (percentage) of aging transcriptome by LTDR or STDR in different tissues, calculated on the basis of the PCA plot (see also Figure S1B and STAR Methods).

(F) Number of differentially expressed genes (DEGs) in LTDR and STDR with opposite direction of aging ($p_{adj} < 0.05$ in both aging and LT/STDR); total number of genes in the dataset = 22,546 (supplemental information).

(G) Number of DEGs rescued by DR (old versus DR) and the total number of DEGs in aging (young versus old) ($p_{adj} < 0.05$). Total number of genes in the dataset = 22,546 (Table S1).

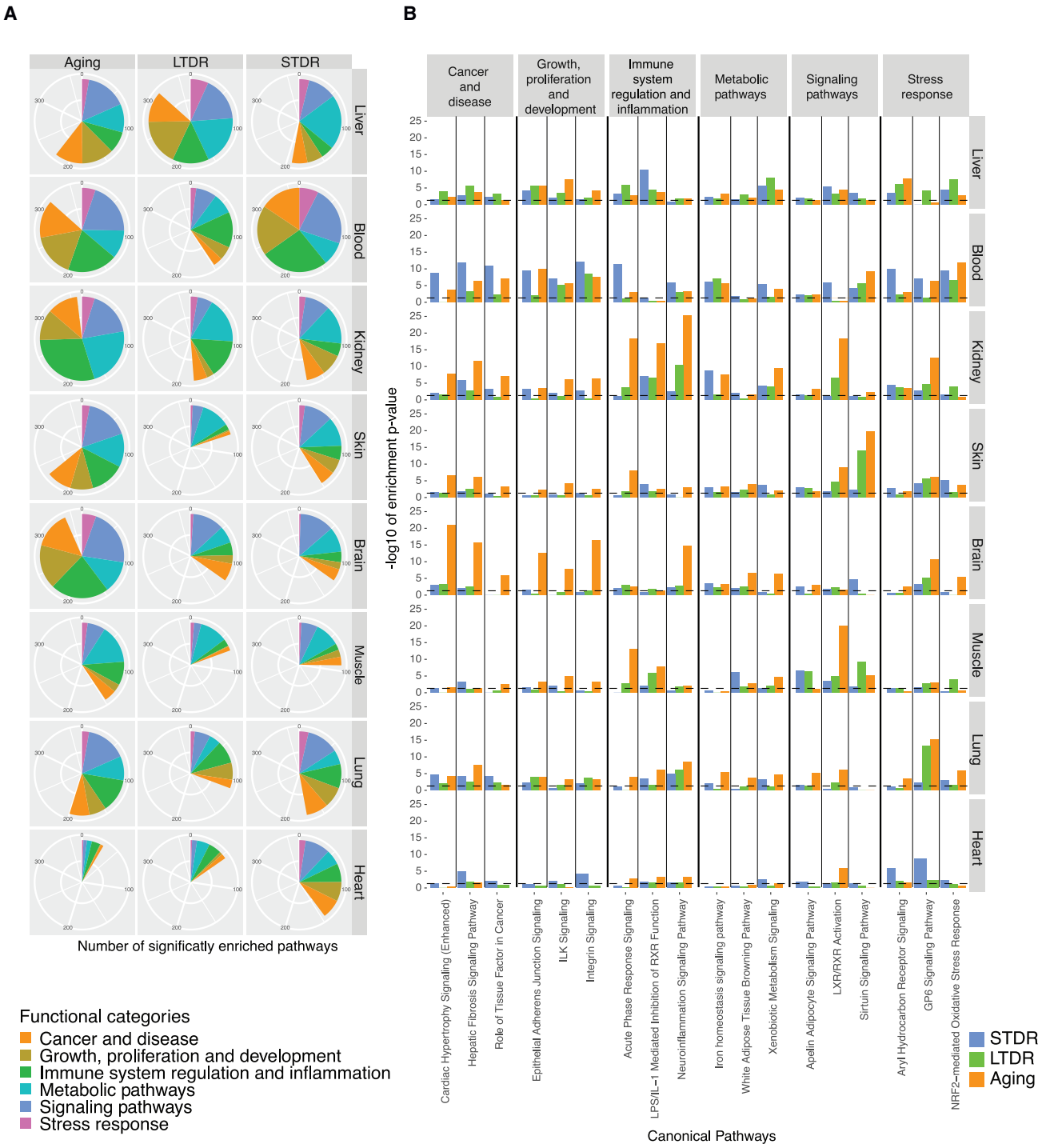

Figure 2. Canonical pathways affected by aging, LTDR, and STDR

(A) Number of differentially regulated canonical pathways significantly enriched in aging (young versus old), LTDR (LTDR versus old), and STDR (STDR versus old) (enrichment p value <0.05). Each pathway is assigned to one of six cellular functions shown by color.

(B) Three examples of the canonical pathway belonging to each functional group. The y axis shows the $-\log_{10}$ of enrichment p value.

system; however, metabolic pathways were the main enriched category in liver, which reflects the importance of the liver in metabolism (Figure 2A). In addition, the functional difference between the response to LTDR and STDR was tissue specific. For instance, both LTDR and STDR altered a similar number of metabolic pathways in liver; in contrast, much fewer inflammatory and

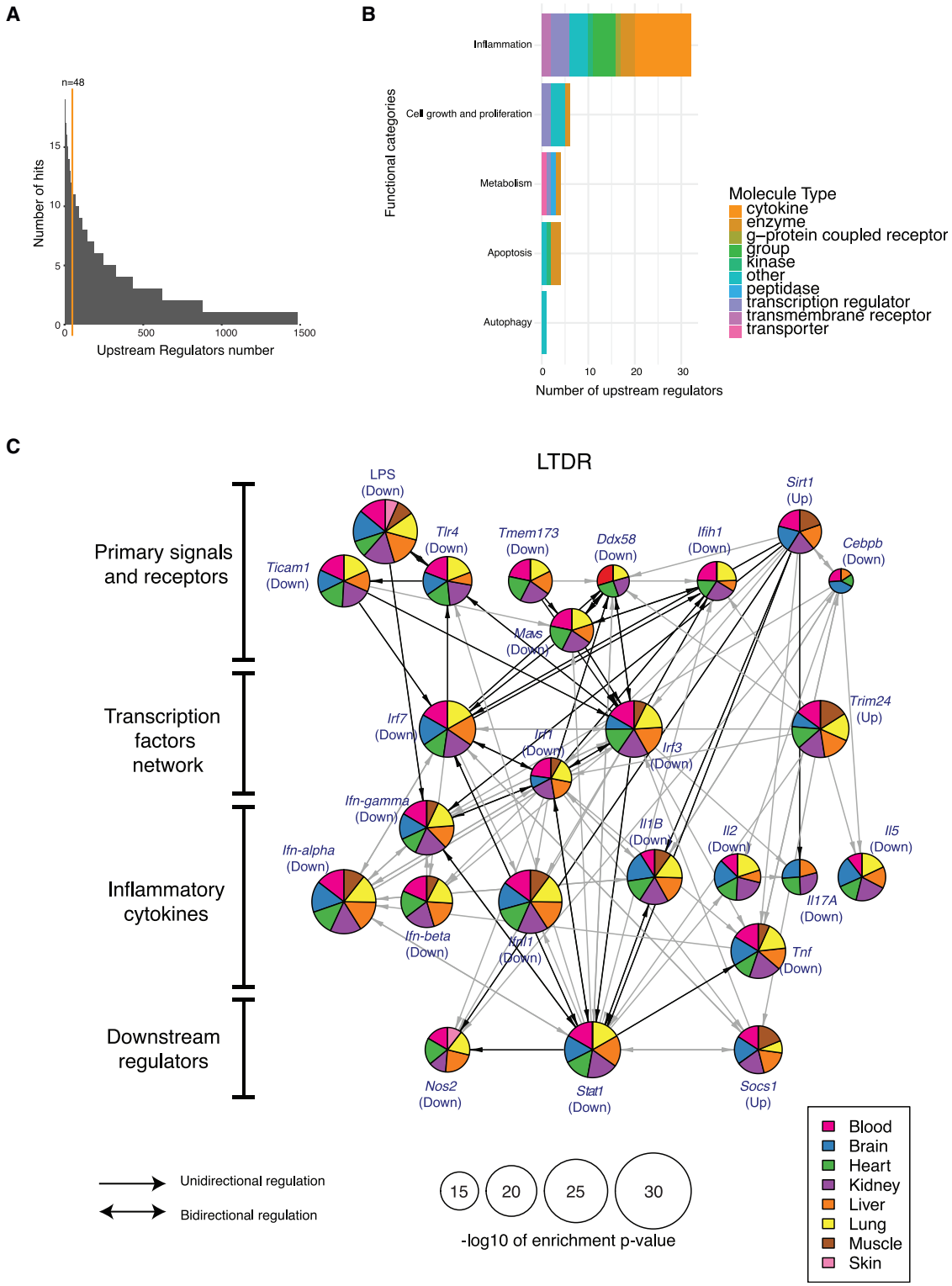

Figure 3. Top common upstream regulators reveal the multi-tissue gene network regulating the inflammation in aging and DR

(A) Histogram shows the number of conditions (8 tissues with 3 conditions each = 24 conditions in total) each upstream regulator significantly changed in the activity prediction (activation *Z* score >2 or less than −2). The x axis shows the number of upstream regulators and the y axis shows the number of conditions with significant changes in the predicted activity. Forty-eight upstream regulators have at least 12 hits out of 24 conditions (orange line) (Table S2).

(legend continued on next page)

signaling pathways were affected in the STDR compared with the LTDR. The transcriptional difference between tissues induced by aging, LTDR, and STDR was not limited to the main functional categories but also at single molecular pathway level. For instance, GP6 signaling in lung, liver X receptor/retinoid X receptor activation in muscle, Sirtuin signaling in skin, inflammatory pathways in kidney, and integrin signaling in blood were highly enriched in both aging and DR (Figure 2B).

Taken together, these data indicated that each tissue is responding quite differently to aging, LTDR, and STDR. In addition, the beneficial effects of LTDR and STDR are different and some tissues respond better to the LTDR while others respond better to STDR. In addition, the results suggested the relevance of inflammation in aging and DR, with some of the inflammatory pathways being the most commonly enriched between different tissues and conditions.

A multi-tissue molecular network regulates inflammation in aging and DR

To better characterize the molecular networks regulating transcriptional alteration in aging and DR, we performed an upstream regulator activity prediction using Ingenuity Pathway Analysis (IPA). IPA software uses a comprehensive literature-based database of known target molecules for each upstream regulator with the direction of regulation (inhibition or activation) to predict the activity of the upstream regulator using the expression of the target genes (Krämer et al., 2014). We did upstream regulator prediction analysis (Table S2), using DEGs from the three comparisons and in eight tissues (old versus young, LTDR versus old, and STDR versus old, a total of 24 conditions). Out of 1,500 upstream regulators, which were predicted to be activated or inhibited significantly (activity Z score > |2|), 48 upstream regulators were predicted to change at least in half of the conditions (in 12 conditions out of 24, Figure 3A). Interestingly, most of these upstream regulators belonged to the inflammatory-related pathways, which highlighted the importance of inflammation in regulating common cellular processes among the different tissues in response to aging and DR (Figure 3B). By using the more enriched upstream regulators, we built up a connection-based network (inflammatory gene network) that was predicted to be perturbed in all of the tissues (except skin) and in all of the conditions (Figures 3C and S2).

The proposed inflammatory gene network (Figures 3C and S2) consists of four main gene layers. The first layer is the primary signals and receptors, which either initiate or regulate the inflammatory signaling. We found the LPS (lipopolysaccharide)/*Tlr4* (Toll-like receptor 4), the *Ddx58* (DExD/H-box helicase 58)/*Ifih1* (Interferon induced with helicase C domain 1)/*Tmem173* (Transmembrane protein 173), and *Sirt1* (Sirtuin 1)/*Cebpb* (CCAAT Enhancer binding protein β) upstream regulators to be strongly enriched on this level. This may indicate that an antigen-mediated (bacterial/viral and/or damaged mitochondrial DNA) response may represent one of the triggering events driving the inflammaging phenomenon. *Sirt*/*Cebp* pathways that are directly affected during DR treatments (Bordone et al., 2007; Ma et al., 2020) may represent the linking pathway between inflammation and metabolism. Second, a network of transcription factors (TFs), such as the members of the *Irf* (interferon regulatory factor) gene family and cytokines such as *Ifn* (interferon) genes and other *Il*s (interleukin), connects the input signals to the downstream gene pathways. One of the well-known downstream regulators of the inflammatory cascade is *Stat1* (Signal transducer and activator of transcription 1), a TF that acts as master regulator of *Ifn* signaling (Ramana et al., 2000). These data indicated that the most affected inflammation pathways that are dysregulated by aging and rescued by DR treatments in multiple tissues are mediated by the *Tlr*/*Ddx58*/*Ifih1*-*Irf*/*Ifn*-*Stat1* axis.

Innate immune system receptors trigger the inflammatory network in aging, which is rescued by DR

Bacterial LPS is an example of an external stimulator that can trigger the immune response. It has been shown that aging increases circulating bacterial endotoxins (such as LPS) (Kim et al., 2016; Thevaranjan et al., 2017) that induce a systemic inflammatory response (Kim et al., 2016), and DR is able to reduce it effectively (Zhang et al., 2013; Pan et al., 2018). In agreement with the previous studies, in our RNA-seq data LPS was predicted to be an active upstream regulator during aging and inhibited by both short- and long-term DR in all tissues, except STDR in skin (Figure 4A). ELISA assay revealed endotoxin increase in the blood serum of old mice, but not of old mice in STDR (Figure S3A) as previously reported (Pan et al., 2018).

Using known genes that are regulated during inflammatory response (445 genes differentially expressed at least in one tissue/condition extracted from IPA), we defined an inflammatory response gene set. Based on our analysis, inflammatory response increased in aging and decreased in DR in all of the studied tissues, except skin and STDR in muscle (Figure 4B). Skin showed completely opposite behavior with decreasing inflammatory response in aging and increasing response by both LTDR and STDR (Figure 4B). In muscle, LTDR was able to rescue the inflammation induced by aging; however, STDR increased the inflammatory response (Figure 4B). These exceptions can be explained by the bacterial endotoxin receptor expression. LPS and other types of bacterial endotoxins are recognized by several innate immune system receptors and molecular complexes, although the most important and well-known receptor is the *Tlr* gene family (specially *Tlr4*) (Mazgaeen and Gurung, 2020). With a few exceptions, the expression of *Tlr4* was

(B) The functional category of the top common 48 upstream regulators (A). The x axis shows the number of upstream regulators and the y axis shows the functional category.

(C) The proposed network of upstream regulators regulating the inflammation in LTDR. Each circle shows an upstream regulator. The size of the circle shows the sum of $-\log_{10}$ of enrichment p value for all of the tissues specified by the colors in each node. Each circle is a pie chart showing the contribution of different tissues in the sum of the $-\log_{10}$ p values. Tissues with non-significant p value (<0.05) or with opposite direction compared with the majority have not been used in the pie chart and calculations. Direction of the activity prediction is shown in parentheses under the name of each upstream regulator. The more relevant molecular connections with the discussed topics are highlighted in black.

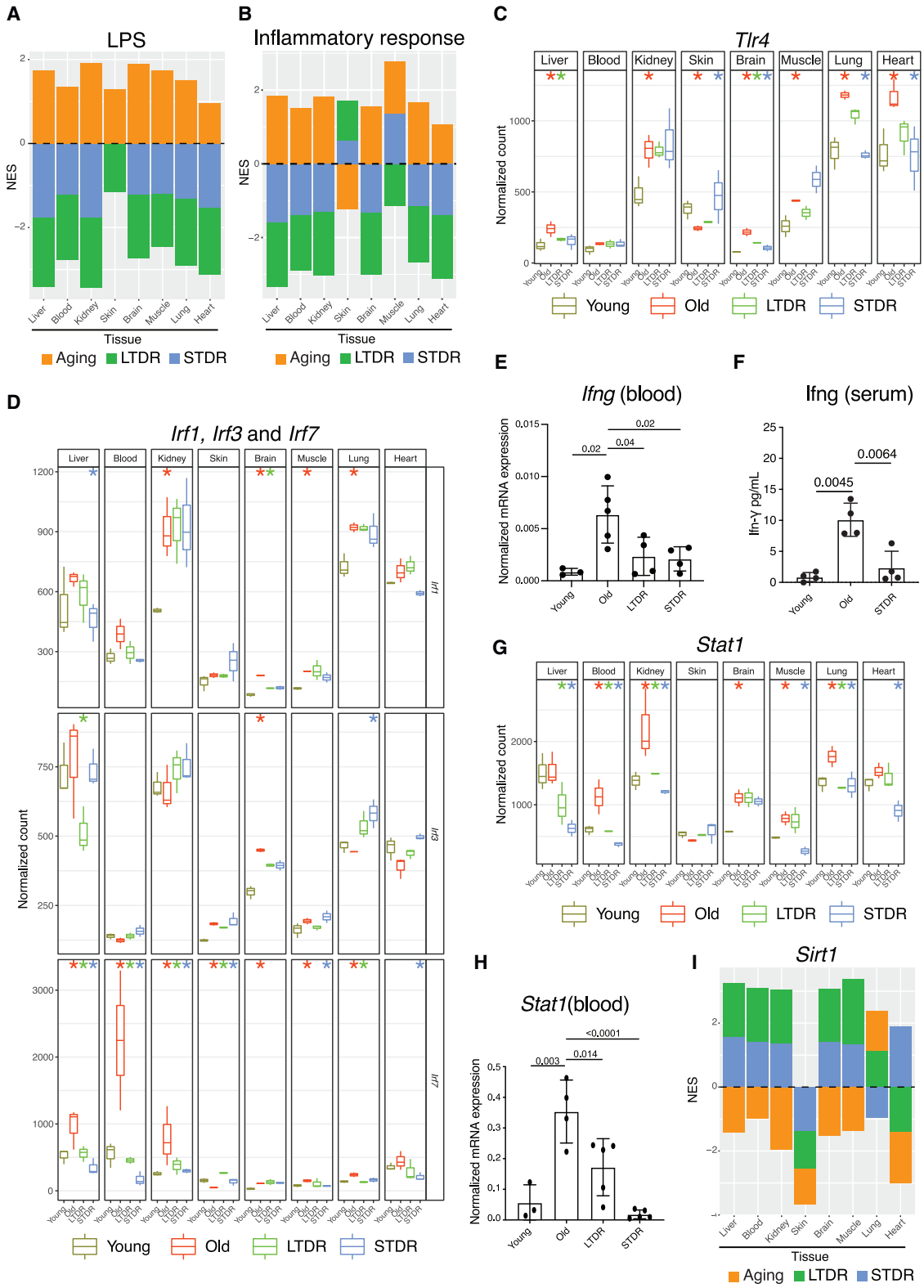

(legend on next page)

upregulated in aging and downregulated in DR (Figure 4C). Surprisingly, skin showed completely the opposite, with *Tlr4* expression downregulated in aging and upregulated in DR. In addition, STDR in muscle increased the expression of *Tlr4*. We suggest that different *Tlr4* expression patterns of skin and STDR in muscle can explain different inflammatory responses in these two tissues.

Tlr4 is one of the most expressed genes among other *Tlr* gene family members in different tissues; however, with some exceptions, other *Tlr* genes also showed similar behavior with increasing expression in aging and decreasing expression upon DR (Figure S3B). For instance, *Tlr13*, which detects bacterial 23S rRNA (Oldenburg et al., 2012), was upregulated in aging and downregulated upon DR in blood, kidney, lung, and heart. Other examples are *Tlr7* and *Tlr8*, which are mainly expressed in lung, detecting pathogen nucleic acids (Forsbach et al., 2008). Similarly, *Tlr7* and *Tlr8* expression increased in aging and decreased upon DR treatment (Figure S3B).

Besides bacterial endotoxins, viral antigen can also stimulate the innate immune response receptors. Viral nucleic acid can be detected by *Ifih1* and *Ddx58*. In addition, *Tmem173* (*Sting1*) detects cytosolic DNA from bacteria or viruses as well as damaged mitochondria (Li et al., 2021). Like *Tlr4*, the expression of *Ifih1*/*Ddx58*/*Tmem173* receptors was differentially upregulated in aging and downregulated upon DR treatment in a tissue- and condition-specific manner (Figure S3C). For example, *Ddx58* and *Tmem173* were significantly changing in muscle aging (upregulation) and DR (downregulation); however, change in *Ifih1* expression was relatively low in muscle. Taken together, these data suggested that many innate immune system receptors, detecting pathogenic antigens and/or damaged mitochondria, are upregulated in aging, potentially leading to higher inflammatory response. DR can effectively downregulate the expression and the activity of these receptors.

DR inhibits the age-induced interferon response

In mammals, *Ifn*s protect the host from viral and non-viral pathogens. Transcriptional initiation of *Ifn* genes depends on the recognition of pathogenic signal (e.g., by *Tlr* family, *Ifih1*, *Tmem173*, and *Ddx58*) that leads to activation of the *Irf* TF family (Honda and Taniguchi, 2006). In our study, *Irf1*, *Irf3*, and *Irf7* were predicted to be activated in aging and inhibited by DR (Figure S3C). These factors were also transcriptionally regulated in a tissue- and condition-specific manner (Figure 4D). For instance, in liver, *Irf1* was significantly downregulated in STDR and *Irf3* in LTDR. *Irf7* was the most expressed gene compared with the others, especially in liver, blood, and kidney. It was significantly upregulated in aging and downregulated in both short- and long-term DR to the young level or even lower (Figure 4D).

Upon expression and/or activation, *Irf* genes induce the expression of the interferon family, like *Ifng* that, in turn, can activate a positive feedback loop (Kang et al., 2002). Based on the target genes, *Ifng* was predicted to be activated upon aging and inhibited in DR in all of the studied tissues except skin (Figure S3E). Our RNA-seq data showed that the expression of *Ifng* in blood increased during aging and decreased upon DR (data not shown), and we further validated this by qRT-PCR (Figure 4E). Ifng protein concentration in blood serum was found in the old animals, but was not detectable in the young and STDR groups of mice (Figure 4F). Ifna and Ifnb was instead not or barely found in the blood serum of all three groups of mice (Figures S3F and S3G). To confirm the systemic activity of Ifng, we measured the expression of *Fcgr1*, a known target of Ifng (Sivo et al., 1996; Famulski et al., 2006), in liver and kidney. *Fcgr1* expression followed the similar pattern of *Ifng* with upregulation in aging and downregulation upon DR (Figures S3H and S3I). These data suggest that old mice have a high systemic activity of *Ifng* that is lost upon either LTDR or STDR.

Tnf is another example of a pro-inflammatory cytokine that was dysregulated by aging and rescued by DR. Tnf is a well-known and particularly interesting inflammatory cytokine that regulates cell proliferation, cell death, and morphogenesis and is involved in many human diseases from depression to cancer (Dowlati et al., 2010; Vanamee and Faustman, 2018). In agreement with previous studies (Spaulding et al., 1997), our RNA-seq data showed that *Tnf* expression is upregulated during aging and downregulated by DR in most of the tissues (Figure S4A).

Stat1 is an essential component of interferon signaling, which mediates several cellular functions, including cell cycle and

Figure 4. DR rescues aging-induced upregulation of innate immunity receptors and activation of interferon response

(A) Activity prediction (gene set enrichment analysis [GSEA]) based on the LPS target genes. The y axis shows the normalized enrichment score (NES). Positive values predict activation (enrichment) and negative values predict inhibition (depletion). For the aging group, young is compared with old, and for LTDR and STDR groups, the DR is compared with the old group. The condition that is not in the plot (STDR, skin) showed neither enrichment nor depletion.

(B) Normalized enrichment score (NES), calculated on the basis of the inflammatory response gene set (545 DEGs in different tissues/condition categorized as the marker of inflammatory response in IPA).

(C) *Tlr4* expression in different tissues and conditions. For p-value calculation, old samples are compared with the young, and DR samples are compared with the old. p value is calculated by DESeq2 (see STAR Methods).

(D) *Irf1*, *Irf3*, and *Irf7* expression in different tissues and conditions. For p-value calculation, old samples are compared with the young, and DR samples are compared with the old. p value is calculated by DESeq2.

(E) Expression of *Ifng* in blood measured by qRT-PCR. p value is calculated by two-tailed t test. For each condition we used $\geq$3 mice. Data are presented as mean ± standard deviation (SD) of the values.

(F) Ifng concentration in blood serum measured by ELISA. p value is calculated by two-tailed Welch's t test. Data are presented as mean ± SD of the values from four mice (n = 4).

(G) *Stat1* expression in different tissues (color) and condition (x axis). p value is calculated by DESeq2 comparing old with young and LTDR/STDR with old. *$p < 0.05$.

(H) Expression of *Stat1* in blood measured by qRT-PCR. p value is calculated by two-tailed t test. For each condition we used $\geq$3 mice. Data are presented as mean ± SD of the values.

(I) GSEA of Sirt1 in different tissues (x axis) and conditions (color). The y axis shows normalized enrichment score (NES). p value is calculated by two-tailed t test.

apoptosis, in response to stimulation by different inflammatory cytokines and growth factors (Zhang and Liu, 2017). Based on our analysis, *Stat1* activity was predicted to increase in aging and decrease in DR in all of the studied tissues except skin (Figure S4B). *Stat1* was also transcriptionally regulated in different tissues. *Stat1* was significantly upregulated during aging in blood, kidney, brain, muscle, and lung; importantly, it was downregulated after DR treatment in liver, blood, kidney, and lung both in LTDR and STDR, as well as in muscle and heart in STDR only (Figures 4G and 4H). In the proposed inflammatory network, *Stat1* is regulated by different upstream regulators from the primary signals and receptors to TFs and inflammatory cytokines (Figures 3C and S2). *Stat1* can be activated by *Ifng* (Cossetti et al., 2014), and transcriptionally regulated by *Irf1*, *Irf3*, and *Irf7* (Lazear et al., 2013; Xu et al., 2016) as well as inflammatory cytokines such as *Il1b* (Rivieccio et al., 2005). *Stat1* positively regulates *Tnf* and *Nos2* (Kong et al., 2016). Our data suggest that *Stat1* represents the most enriched downstream player of the inflammatory gene network and propose Stat1 as the master TF finally mediating transcriptional response to the inflammatory cascade in the analyzed tissues (except skin). In summary, our data indicate that during aging, the innate immune system receptors for bacterial or viral endotoxins and nucleic acids are upregulated in most of the tissues of the organism. Their upregulation and/or activation lead to higher inflammatory response through a network of TFs (mainly *Irf1*, *Irf3*, and *Irf7*) and inflammatory cytokines (such as *Ifng*, *Tnf*, and some interleukins) that finally results in higher activity of *Stat1*. In addition, *Sirt1* may connect the metabolic stress response to the inflammaging, as it has been shown to negatively regulate many of these genes (Figures 3C and S2) (Xie et al., 2013). Interestingly, *Sirt1* is predicted to be inhibited in aging and activated upon DR in most of the tissues (Figure 4I), proposing it as one of the major actors responsible for the DR-mediated amelioration of inflammaging.

To verify, at protein level, the up- or downregulation of the main gene network hubs, we performed western blotting analysis of Stat1, Sirt1, Irf3, and Tlr4 in liver and kidney in aging and in the two DR conditions (Figures 5A and S4C). In liver, we validated Tlr4 protein upregulation in aging and downregulation of Irf3, Tlr4, and Stat1 in LTDR and STDR. We also observed a significant reduction of Sirt1 protein in old mice and re-upregulation following DR interventions (Figure 5A). Similarly, in kidney, we observed protein upregulation of Irf3, Tlr4, and Stat1 in aging and downregulation following DR conditions, while Sirt1 showed an inverse pattern (Figure S4C).

To better understand the relative contribution of the tissue-specific cells and of the tissue-resident immune cells to the transcriptional alterations observed in aging and in DR, we performed gene expression analysis in CD45 (marker of immune cells) positive (+) or negative (–) cells. First, we quantified the percentage of the $CD45^+$ cells in three different organs (kidney, liver, and lung) and observed a significant increase of this cell type during aging only in kidney, with no rescue in the STDR mice (Figure 5B). This result indicated that during aging there is an increase of the tissue-resident immune cells, but the DR regime ameliorates the tissue-specific inflammatory state without reducing the number of the infiltrated immune cells. We performed qRT-PCR of the main hubs of the proposed inflammatory gene network (Figures 5C and S4D). We observed an increase of the *Tlr* and *Irf* genes in both $CD45^-$ and $CD45^+$ cells during aging that was rescued in the STDR mice (Figures 5C and S4D). *Stat1* showed a similar trend, but its expression and regulation were stronger in the $CD45^+$ cells. *Ifng* was upregulated in old and rescued in STDR mice in the $CD45^+$ cells of all three tissues, but not detected in the $CD45^-$ cells. Finally, *Sirt1* was downregulated in aging in kidney and in lung (only in the $CD45^+$ cells) (Figures 5C and S4D). Overall, the qRT-PCR experiment confirmed the gene expression pattern identified by the RNA-seq analysis and revealed that the inflammatory gene network involves both tissue-specific cells and tissue-resident immune cells.

Aging induces a general open chromatin rearrangement which is not rescued by DR, except on *Stat1* and *Irf* target genes

To confirm the activity prediction (from RNA-seq data) of the proposed key TFs (Irf1/3/7 and Stat1), we performed the assay for transposase-accessible chromatin using sequencing (ATAC-seq) of kidney and liver, since these two tissues show a big change in the predicted activity of Irf and Stat1 TFs in aging and LTDR. The PCA plot of the ATAC-seq data revealed that aging and LTDR induced changes in the chromatin accessibility and that the samples were clustering in a condition-specific fashion (Figure 6A). Analysis of the ATAC-seq signal intensity on one million of 1 kb random genomic regions showed a loss of signal intensity in the regions that showed high intensity in young animals (Figure 6B, light-blue box). Distribution of the sequenced reads on all genes showed a general decrease of open chromatin around the transcription start site (TSS) and increase in the gene body in old and LTDR mice (Figure 6C for kidney and Figure S5B for liver). A distribution plot of ATAC-seq enriched peaks (p value $<10^{-5}$) with respect to the annotated RefSeq genes, sorted by their expression level, showed a genome-wide enrichment of peaks in the gene bodies and around the TSS of non-/lowly expressed genes in old animals (Figure S5A, kidney). DR was minimally or not rescuing the chromatin accessibility changes caused by aging (Figures 6C and S5B). The histogram of the distribution of the sequenced reads (ATAC-seq reads) covering the promoters (±1 kb of TSS) revealed a bimodal distribution in young animals (Figure 6D for kidney and Figure S5C for liver), suggesting that the two normal distributions could represent open and closed promoters of transcriptionally active and repressed genes. The expression level of the genes associated with these two groups of promoters confirmed that the bimodal distribution reflects the on/off transcriptional state of the genes (Figures 6E and S5D). Of note, during aging the distribution curves of the open and closed chromatin promoters almost completely overlap (Figures 6F and S5E). Importantly, LTDR treatment did not rescue this epigenetic phenotype (Figures 6G and S5F). Finally, plotting of the ATAC-seq signal intensity of genes subdivided into ventiles according to their expression level revealed that aging slightly opens the promoter of the non-/lowly expressed genes and closes the promoter of the highly expressed genes (Figures 6H and S5G). Interestingly, gene expression correlated with these chromatin rearrangements, with a global slight increase of the non-/lowly

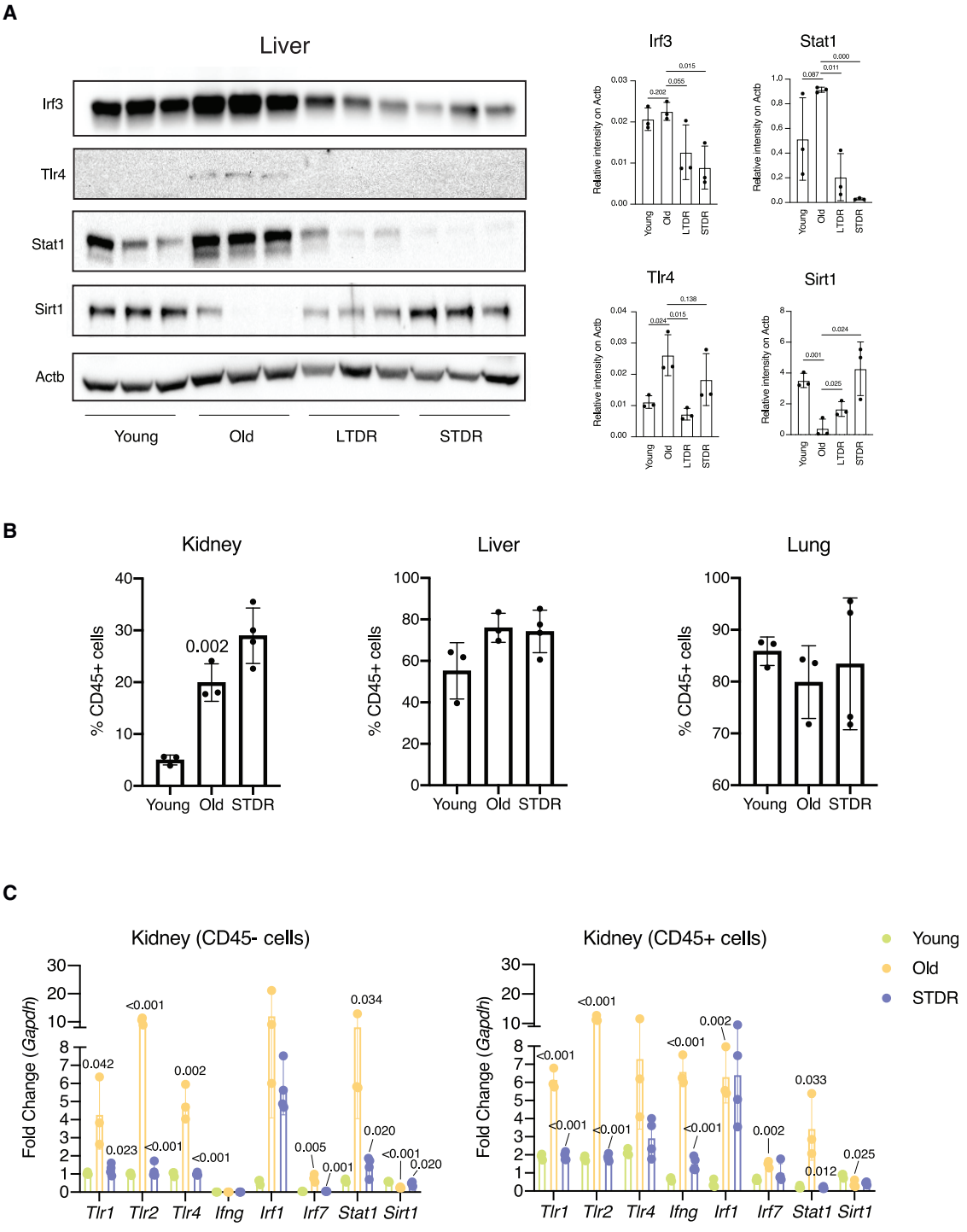

Figure 5. Inflammaging gene network is upregulated at protein level and in both tissue-specific cells and tissue-resident immune cells

(A) Left: western blotting of the indicated protein in the indicated tissue and conditions. Right: quantification of the western blot signals. Bar charts show mean ± SD. p value is calculated by one-tailed Welch's t test. For each condition we used three mice.

(B) FACS analysis of CD45$^-$ and CD45$^+$ cells of kidney, liver, and lung. p value is calculated by two-tailed unpaired Welch's t test between young and old as well as between old and STDR. Only significant comparisons (p values <0.05) are reported. For each condition we used ≥3 mice. Bar charts show mean ± SD.

(C) Bar charts showing the results of the qRT-PCR of the indicated genes in CD45$^-$ and CD45$^+$ cells in kidney. p value is calculated by two-tailed unpaired Welch's t test between young and old as well as between old and STDR. Only significant comparisons (p values <0.05) are reported. For each condition we used ≥3 mice. Bar charts show mean ± SD.

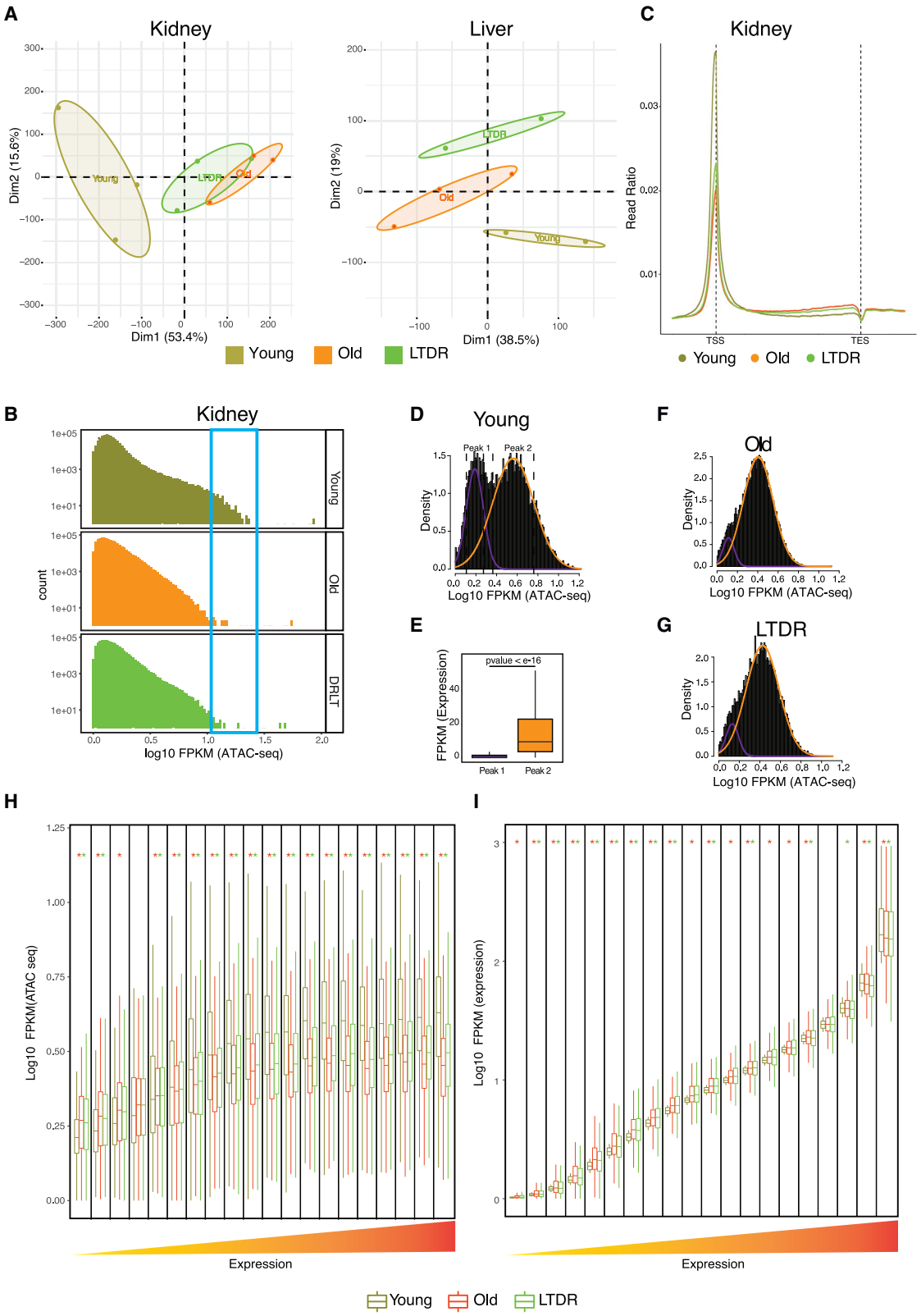

(legend on next page)

expressed genes and decrease of highly expressed genes (Figures 6I and S5H). Again, DR was not able to effectively rescue either the epigenetic or the transcriptional phenotype (Figures 6I and S5H). Taken together, these data showed that aging induces a genome-wide chromatin accessibility alteration, particularly by making closed and open regions, respectively, more open and closed, indicating a blunting of the epigenetic landscape with subsequent increase of transcriptional noise and not fully performing expression of highly transcribed genes. While DR was able to partially rescue DEGs, it did not ameliorate aging-associated global epigenetic alteration nor this latter transcriptional phenotype.

RNA-seq data showed a significant positive enrichment of Stat1 target genes expression in aging (Figures 7A and S6A) and depletion (negative enrichment) in LTDR (Figures 7B and S6B) in both kidney and liver. ATAC-seq data showed that the peaks (p value $<10^{-5}$) with Stat1 binding motif in ±5 kb of TSS of Stat1 target genes had significantly more open chromatin in the old relative to the young, and DR was able to significantly rescue this phenotype in both kidney and liver (Figures 7C and S6C). Similarly, Irf3 and Irf7 had significant positive enrichment of the expression of target genes in aging (Figures 7D, 7G, S6D, and S6G) and depletion in DR (Figures 7E, 7H, S6E, and S6H) as well as more open chromatin in the peaks with corresponding motif in aging and rescue in the DR (Figures 7F, 7I, S6F, and S6I) in both kidney and liver. Figure S7J shows the expression of the top 60 Stat1 target genes, differentially regulated in aging and DR.

In summary, besides the global chromatin accessibility rearrangement observed in aging that was not rescued by DR, aging-associated open chromatin loci bearing Stat1 and Irf3/7 binding motifs were rescued by DR effectively, indicating a proper transcriptional control of the Stat1 and Irf3/7 target genes.

DISCUSSION

From the molecular perspective, aging is a result of accumulation of a wide variety of molecular and cellular damage leading to a gradual decrease of physiological organ function, higher risk of disease and, ultimately, death (Aunan et al., 2016). DR, decreasing the calorie intake without malnutrition, is a non-invasive intervention which can extend the lifespan and/or healthspan in a wide range of organisms, from yeast to worms, flies, rodents, and monkeys (Colman et al., 2009; Fontana et al., 2010). In this study, we showed that aging changed the transcriptome of different tissues and that DR was able to partially rescue the age transcriptome. DR intervention in late life has been recently shown to not provide as beneficial effects as long-life DR in lifespan and healthspan extension (Hahn et al., 2019). For this reason, we compare old mice with mice treated with both a lifetime DR (LTDR) and a short-term DR at late life (STDR). We found that responses to the aging, LTDR, and STDR both in magnitude and functional aspects were tissue specific. LTDR has been previously shown to strongly prevent a pro-inflammatory phenotype in aged white adipose tissue pre-adipocytes, whereas a late-onset DR failed in preventing it (Hahn et al., 2019). Our data show that LTDR was more effective in rescuing inflammaging in liver and kidney (Figure 2A), while STDR mitigated aging-associated activation of inflammatory pathways more effectively in blood; in other tissues both LTDR and STDR prevented the pro-inflammatory phenotype to a similar extent. It is tempting to speculate that different DR treatments may have organ- and tissue-specific benefits or detrimental effects. Indeed, other studies also claimed similar beneficial effects of LTDR and STDR (Robertson and Mitchell, 2013) as well as specific differences in tissue and function (Flanagan et al., 2020).

Aging is characterized by a chronic, low-grade inflammation (also called inflammaging) that represents a risk factor for many aging-associated dysfunctions and diseases (Baylis et al., 2013; Franceschi et al., 2017). Different mechanisms have been proposed to fuel inflammaging. Organ failure and/or tissue damage, metabolic and oxidative stress, DNA damage, impairment of autophagy, microbiome dysbiosis, and barrier dysfunction can lead to higher inflammatory response in aging (Kim et al., 2016; Xia et al., 2016). In contrast, DR improves the stem cell function leading to a better tissue regeneration and repair, reduces the metabolic and oxidative stress and DNA damage, increases autophagy, and improves healthy gut microbiome and barrier function (Mana et al., 2017; Pan et al., 2018; Yu

Figure 6. Aging-induced open chromatin rearrangement results in transcriptional change depending on the basal level of gene expression

(A) PCA plot based on the ATAC-seq data (reads per million of merged 10^{-5} peaks, see STAR Methods) for kidney (left) and liver (right). For each condition we used $\geq$4 mice.

(B) Histogram showing the distribution of open and closed chromatin regions in kidney. The x axis shows the $\log_{10}$ FPKM (fragments per kbp transcripts per million sequenced reads) of sequenced reads (ATAC-seq) covering 1 million random regions (1 kb). The y axis shows the number of regions with respective FPKM.

(C) Relative sequenced read distribution (normalized to the total number of sequenced reads per sample) in respect of the gene annotation in kidney. The dashed lines show the TSS (transcription start site) and the TES (transcription end site). Between the TSS and TES, the position (x axis) is relative to the gene size. Outside of the gene region (before TSS and after TES) the positions are absolute. Averages of the replicates for each group are used in the plot.

(D) Histogram shows the distribution of open chromatin of the promoter regions (±1 kb of TSS of the longest isoform) in kidney of the young group. Modeling of the distribution suggests two normal distributions. Mean ± SD for each normal distribution is shown as a dashed line.

(E) Expression (FPKM) of genes representing each distribution (peaks 1 and 2 represent the violet and orange distribution, respectively in Figure 5D). The p value is calculated by two-tailed Wilcoxon test.

(F and G) Similar to (D), the histogram shows the distribution of open chromatin of the promoter regions in kidney of the old (F) and LTDR (G) group.

(H) Box plot shows the open chromatin intensity ($\log_{10}$ FPKM of ATAC-seq data) in the promoter region of genes with different level of expression in kidney. The genes are sorted based on their expression in the young group (x axis). p value is calculated using two-tailed paired t test for which the $\log_{10}$ FPKM (ATAC-seq) of each gene is compared in different groups. For p-value calculation, the old is compared with the young and the LTDR is compared with the old. *$p < 0.05$.

(I) Box plot shows the expression ($\log_{10}$ FPKM, y axis) of the genes (kidney) with different level of basal expression in young as in Figure 4E. p value is calculated using two-tailed paired t test for which the expression of each gene is compared in different groups. For p-value calculation, the old is compared with the young and the DRLT is compared with the old. *$p < 0.05$.

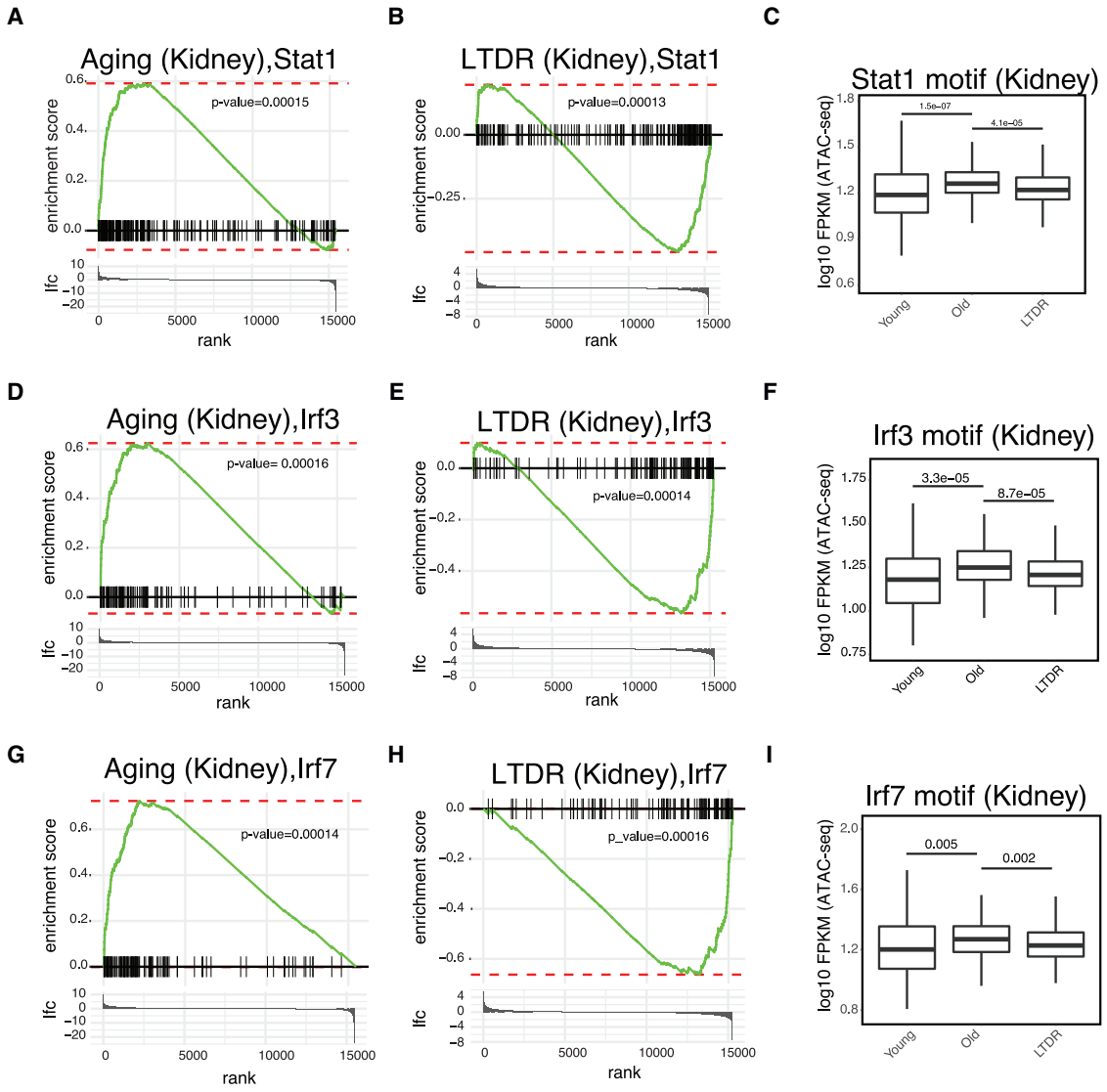

Figure 7. ATAC-seq and RNA-seq data confirm the activation of Irf3, Irf7, and Stat1 transcription factors in aging and inhibition by DR in kidney

(A and B) GSEA of the Stat1 target gene expression in young versus old (A) and old versus LTDR (B) comparisons in kidney. Stat1 target gene expression is positively enriched in old (compared with the young) and negatively enriched in LTDR (compared with the old).

(C) Open chromatin intensity (log_{10} FPKM, ATAC-seq data) of the peaks ($p < 10^{-5}$, merging of all replicates, see STAR Methods) ± 5 kb of TSS of the Stat1 target genes with the Stat1 binding motif in kidney. p value is calculated with paired t test, comparing the same genes in old versus young and LTDR versus old.

(D and E) GSEA of the Irf3 target gene expression in young versus old (D) and old versus LTDR (E) comparisons (similar to A and B) in kidney.

(F) Open chromatin intensity of Irf3 target genes with the Irf3 binding motif in kidney (similar to C).

(G and H) GSEA of the Irf7 target gene expression in young versus old (D) and old versus LTDR (E) comparisons (similar to A and B) in kidney.

(I) Open chromatin intensity of Irf7 target genes with the Irf7 binding motif in kidney (similar to F).

et al., 2020). Our data show that both LTDR and STDR ameliorate inflammaging at the systemic level on almost all levels of aging-associated inflammatory signaling hyperactivation.

From a molecular perspective, different tissue-specific molecular networks and signaling pathways are reported to be involved in the inhibition of inflammation by DR. For instance, inhibition of nuclear factor κB and AP-1 in kidney (Jung et al., 2009), and inhibition of the PI3K/AKT pathway in skeletal muscles (Mercken et al., 2013), have been observed. However, a multi-tissue approach to systematically assess the relationship between aging, DR, and inflammation has never been performed thus far. Here we suggested that aging leads to upregulation and/or activation of innate immune response receptors, leading to the activation of interferon response through the Irf TF family. The activation of interferon response leads to higher production of inflammatory cytokines (such as Ifng) and activation of Stat1. We also show that DR can effectively reduce this inflammatory gene network.

Different mechanisms can be suggested to explain how aging induces higher expression and/or activation of the innate immune response receptor and how DR can rescue it. For example, to compensate immunosenescence, the innate immune response becomes more activated, which induces the pro-inflammatory profile (Dulken et al., 2019; Salminen et al., 2008), and it has been shown that DR improves the adoptive immune response and decline in immunosenescence (Longo and Cortellino, 2020; Ma et al., 2020). In agreement with the recent study on rats, we also observed that DR attenuated aging-related changes in gene expression and the aging-associated increase of the pro-inflammatory phenotype (Ma et al., 2020). In addition, aging induces gut microbiome dysbiosis and barrier dysfunction, leading to a higher systemic level of bacterial endotoxins (Kim et al., 2016; Thevaranjan et al., 2017), and DR improves the healthy gut microbiome and increases barrier function (Zhang et al., 2013; Pan et al., 2018). Indeed, our RNA-seq data predicted a higher exposure of different tissues to the LPS in aging which was rescued by DR, suggesting that the reduction of inflammaging mediated by DR may be caused by its impact on the gut microbiome/permeability. We observed that inflammatory response was more activated during aging and inhibited by DR in all of the studied tissues except skin. Interestingly, we observed that in skin most of the studied innate immune receptors were either not changing or decreasing in aging and increasing in DR (contrarily to the other tissues). This opposite skin phenotype should be further investigated. Besides the *Tlr* gene family that recognizes pathogen antigens, Ifih1, Ddx58, and Tmem173 are the other type of receptors that detect pathogenic nucleic acid and showed regulation similar to that of *Tlr* genes. In addition, Tmem173 (Sting1) can detect mitochondrial DNA in cytosol (Li et al., 2021). Interestingly, muscle showed a significant increase of the expression of Tmem173 in aging and downregulation in DR. In addition, the most affected pathways in aging of muscle were oxidative phosphorylation and mitochondrial dysfunction (data not shown), which may suggest the importance of mitochondrial damage in activation of Tmeme173. Regardless of systemic level of bacterial and/or viral endotoxins as well as mitochondrial damage, upregulation of the innate immune response receptors in aging can lead to a higher inflammatory response, which is diminished by DR.

The suggested inflammatory gene network can regulate different cellular processes mainly through the Irf and Stat1 TFs. Both RNA-seq and ATAC-seq data showed that the expression and the activity of TFs increased in aging and decreased in DR in most of the tissues. In agreement with our results, a previous study showed that there is a significant positive correlation between age and the expression of *Stat1* in human blood leukocytes (Harries et al., 2011). In addition, it has been shown that *Stat1* expression in rat brain increases significantly in aging (Moyse et al., 2012). Furthermore, ATAC-seq data suggested a general chromatin accessibility rearrangement, with an opening of the close chromatin and closing of the open chromatin regions in the genome. As a consequence, we observed upregulation of the non-/lowly expressed genes and downregulation of the highly expressed genes. Of note, while DR was not able to reverse this global epigenetic alteration, it succeeded in rescuing chromatin accessibility on Irf and Stat1 target regions, indicating that DR can epigenetically and transcriptionally ameliorate the pro-inflammatory phenotype.

In summary, using transcriptional profiling (RNA-seq), we suggested a multi-tissue molecular network that regulates inflammaging. We showed that during aging, upregulation of the innate immune system receptor induced the activation of interferon response, including the interferon regulatory factors (*Irf*), leading to the transcription of different inflammatory cytokines such as interferon-γ and regulation of different cellular processes through Stat1 (Figure 7). This inflammaging gene network is rescued by DR interventions. Our study complements and expands the study performed on a rat model (Ma et al., 2020) by characterizing the inflammatory network at gene and signaling pathway level in a different mammalian model and following two very different (short- and long-term) DR interventions. In addition, ATAC-seq data confirm the activity of the key transcription regulators of the network. Our results improve our knowledge of the molecular mechanism of inflammation in aging and DR. This study provides targets for therapeutic approaches aimed at reducing inflammaging.

Limitations of the study

Our study was performed by using C57BL/6J mice. A previous study showed that, in some mouse strains, DR fails to extend the lifespan (Liao et al., 2010). It would be interesting to analyze whether DR does not modulate inflammaging in these mouse strains.

STAR★METHODS

Detailed methods are provided in the online version of this paper and include the following:

- KEY RESOURCES TABLE
- RESOURCE AVAILABILITY
  - Lead contact
  - Materials availability
  - Data and code availability
- EXPERIMENTAL MODEL AND SUBJECT DETAILS
  - Mice
- METHOD DETAILS
  - Dietary restriction
  - Sample collection
  - Mouse serum collection
  - ELISA detection
  - Flow cytometry
  - Total RNA sequencing library preparation
  - Reverse transcription and real-time qPCR
  - Western Blot
  - Preparation of recombinant Tn5 transposase
  - ATAC-seq library preparation
- QUANTIFICATION AND STATISTICAL ANALYSIS
  - RNA-seq data analysis
  - ATAC-seq data analysis
- ADDITIONAL RESOURCES
  - Ethics statement

SUPPLEMENTAL INFORMATION

Supplemental information can be found online at https://doi.org/10.1016/j.celrep.2022.111017.

ACKNOWLEDGMENTS

This work was supported by funding from the Leibniz Institute on Aging (FLI) and Alexander von Humboldt Foundation. The authors are grateful for the support to the Animal House at the Leibniz Institute on Aging – Fritz Lipmann Institute.

AUTHOR CONTRIBUTIONS

F.A., S.M.M.R., A.O., K.L.R., and F.N. conceived and designed the experiments. S.M.M.R., F.A., and F.N. wrote the manuscript with contributions from all the authors. F.A. performed the RNA-seq library preparation. F.A. performed ATAC-seq library preparation with support from S.H. and T.P.J. S.N., A.K., N.G., G.D., and F.A. collected the tissues and performed qRT-PCR, western blot, and ELISA assay. S.M.M.R. and F.N. analyzed the data.

DECLARATION OF INTERESTS

The authors declare no competing interests.

Received: December 24, 2020
Revised: March 28, 2022
Accepted: June 7, 2022
Published: June 28, 2022

REFERENCES

Anders, S., Pyl, P.T., and Huber, W. (2015). HTSeq-a Python framework to work with high-throughput sequencing data. Bioinformatics *31*, 166–169. https://doi.org/10.1093/bioinformatics/btu638.

Arends, J., Bachmann, P., Baracos, V., Barthelemy, N., Bertz, H., Bozzetti, F., Fearon, K., Hütterer, E., Isenring, E., Kaasa, S., et al. (2017). ESPEN guidelines on nutrition in cancer patients. Clin. Nutr. *36*, 11–48. https://doi.org/10.1016/j.clnu.2016.07.015.

Aunan, J., Watson, M.M., Hagland, H.R., and Soreide, K. (2016). Molecular and biological hallmarks of ageing. Br. J. Surg. *103*, e29–e46. https://doi.org/10.1002/bjs.10053.

Barzilai, N., Huffman, D.M., Muzumdar, R.H., and Bartke, A. (2012). The critical role of metabolic pathways in aging. Diabetes *61*, 1315–1322. https://doi.org/10.2337/db11-1300.

Baylis, D., Bartlett, D.B., Patel, P.H., and Roberts, C.H. (2013). Understanding how we age: insights into inflammaging. Longev. Healthspan *2*, 2–8. https://doi.org/10.1186/2046-2395-2-8.

Benaglia, T., Chaveau, D., Hunter, D., and Young, D. (2009). mixtools: an R package for analyzing finite mixture models. J. Stat. Softw. *32*, 1–29. https://doi.org/10.18637/jss.v032.i06.

Bordone, L., Cohen, D., Robinson, A., Motta, M.C., van Ven, E., Czopik, A., Steele, A.D., Crowe, H., Marmor, S., Luo, J., et al. (2007). SIRT1 transgenic mice show phenotypes resembling calorie restriction. Aging Cell *6*, 759–767. https://doi.org/10.1111/j.1474-9726.2007.00335.x.

Colman, R.J., Anderson, R.M., Johnson, S.C., Kastman, E.K., Kosmatka, K.J., Beasley, T.M., Allison, D.V., Cruzen, C., Simmons, H.A., Kemnitz, J.W., and Weindruch, R. (2009). Caloric restriction delays disease onset and mortality in rhesus monkeys. Science *325*, 201–204. https://doi.org/10.1126/science.1173635.

Cossetti, C., Iraci, N., Mercer, T.R., Leonardi, T., Alpi, E., Drago, D., Alfaro-Cervello, C., Saini, H.K., Davis, M.P., Schaeffer, J., et al. (2014). Extracellular vesicles from neural stem cells transfer IFN-γ via Ifngr1 to activate Stat1 signaling in target cells. Mol. Cell *56*, 193–204. https://doi.org/10.1016/j.molcel.2014.08.020.

Das, S.K., Roberts, S.B., Bhapkar, M.V., Villareal, D.T., Fontana, L., Martin, C.K., Racette, S.B., Fuss, P.J., Kraus, W.E., Wong, W.W., et al. (2017). Body-composition changes in the Comprehensive Assessment of Long-term Effects of Reducing Intake of Energy (CALERIE)-2 study: a 2-y randomized controlled trial of calorie restriction in non-obese humans. Am. J. Clin. Nutr. *105*, 913–927. https://doi.org/10.3945/ajcn.116.137232.

Dirks, A.J., and Leeuwenburgh, C. (2006). Caloric restriction in humans: potential pitfalls and health concerns. Mech. Ageing Dev. *127*, 1–7. https://doi.org/10.1016/j.mad.2005.09.001.

Dowlati, Y., Herrmann, N., Swardfager, W., Liu, H., Sham, L., Reim, E.K., and Lanctot, K.L. (2010). A meta-analysis of cytokines in major depression. Biol. Psychiatry *67*, 446–457. https://doi.org/10.1016/j.biopsych.2009.09.033.

Dulken, B.W., Buckley, M.T., Negredo, P.N., Saligrama, N., Cayrol, R., Leeman, D.S., George, B.M., Boutet, S.C., Hebestreit, K., Pluvinage, J.V., et al. (2019). Single-cell analysis reveals T cell infiltration in old neurogenic niches. Nature *571*, 205–210. https://doi.org/10.1038/s41586-019-1362-5.

Famulski, K.S., Einecke, G., Reeve, J., Ramassar, V., Allanach, K., Mueller, T., Hidalgo, L.G., Zhu, L.F., and Halloran, F.P. (2006). Changes in the transcriptome in allograft rejection: IFN-γ-induced transcripts in mouse kidney allografts. Am. J. Transplant. *6*, 1342–1354. https://doi.org/10.1111/j.1600-6143.2006.01337.x.

Flanagan, E.W., Most, J., Mey, J.Y., and Redman, L.M. (2020). Calorie restriction and aging in humans. Annu. Rev. Nutr. *40*, 105–133. https://doi.org/10.1146/annurev-nutr-122319-034601.

Fontana, L., Partridge, L., and Longo, V.D. (2010). Extending healthy life span—from yeast to humans. Science *328*, 321–326. https://doi.org/10.1126/science.1172539.

Fontana, L., and Partridge, L. (2015). Promoting health and longevity through diet: from model organisms to humans. Cell *161*, 106–118. https://doi.org/10.1016/j.cell.2015.02.020.

Forsbach, A., Nemorin, J.G., Montino, C., Müeller, C., Samulowitz, U., Vicari, A.P., Jurk, M., Mutwiri, G.K., Krieg, A.M., Lipford, G.B., and Vollmer, J. (2008). Identification of RNA sequence motifs stimulating sequence-specific TLR8-dependent immune responses. J. Immunol. *180*, 3729–3738. https://doi.org/10.4049/jimmunol.180.6.3729.

Franceschi, C., Garagnani, P., Vitale, G., Capri, M., and Salvioli, S. (2017). Inflammaging and 'Garb-aging'. Trends Endocrinol. Metab. *28*, 199–212. https://doi.org/10.1016/j.tem.2016.09.005.

Hahn, O., Drews, L.F., Nguyen, A., Tatsuta, T., Gkioni, L., Hendrich, O., Zhang, Q., Langer, T., Pletcher, S., Wakelam, M.J.O., et al. (2019). A nutritional memory effect counteracts the benefits of dietary restriction in old mice. Nat. Metab. *1*, 1059–1073. https://doi.org/10.1038/s42255-019-0121-0.

Harries, L.W., Hernandez, D., Henley, W., Wood, A.R., Yaghootkar, H., Dutta, A., Murray, A., Frayiling, T.M., Guralnik, J.M., Bandinelli, S., et al. (2011). Human aging is characterized by focused changes in gene expression and deregulation of alternative splicing. Aging Cell *10*, 868–878. https://doi.org/10.1111/j.1474-9726.2011.00726.x.

Heinz, S., Benner, C., Spann, N., Bertolino, E., Lin, Y.C., Laslo, P., Cheng, J., Murre, C., Singh, H., and Glass, C.K. (2010). Simple combinations of lineage-determining transcription factors prime cis-regulatory elements required for macrophage and B cell identities. Mol. Cell *38*, 576–589. https://doi.org/10.1016/j.molcel.2010.05.004.

Hennig, B.P., Velten, L., Racke, I., Tu, C.S., Thoms, M., Rybin, V., Besir, H., Remans, K., and Steinmetz, L.M. (2018). Large-scale low-cost NGS library preparation using a robust Tn5 purification and tagmentation protocol. G3 (Bethesda) *8*, 79–89. https://doi.org/10.1534/g3.117.300257.

Honda, K., and Taniguchi, T. (2006). IRFs: master regulators of signalling by Toll-like receptors and cytosolic pattern-recognition receptors. Nat. Rev. Immunol. *6*, 644–658. https://doi.org/10.1038/nri1900.

Jung, K., Lee, E.K., Kim, J.Y., Zou, Y., Sung, B., Heo, H.S., Kim, M.K., Lee, J., Kim, N.D., Yu, B.P., and Chung, H.-Y. (2009). Effect of short-term calorie restriction on pro-inflammatory NF-kB and AP-1 in aged rat kidney. Inflamm. Res. *58*, 143–150. https://doi.org/10.1007/s00011-008-7227-2.

Kang, D.C., Gopalkrishnan, R.V., Wu, Q., Jankowsky, E., Pyle, A.M., and Fisher, P.B. (2002). mda-5: an interferon-inducible putative RNA helicase with double-stranded RNA-dependent ATPase activity and melanoma growth-suppressive properties. Proc. Natl. Acad. Sci. USA. *99*, 637–642. https://doi.org/10.1073/pnas.022637199.

Kazemi, A., Speakman, J.R., Soltani, S., and Djafarian, K. (2020). Effect of calorie restriction or protein intake on circulating levels of insulin like growth factor I in humans: A systematic review and meta-analysis. Clin Nutr *93*, 1705–1716. https://doi.org/10.1016/j.clnu.2019.07.030.

Kim, K.A., Jeong, J.J., Young Yoo, S., and Kim, D.H. (2016). Gut microbiota lipopolysaccharide accelerates inflammaging in mice. BMC Microbiol. *16*. https://doi.org/10.1186/s12866-016-0625-7.

Kong, D., Shen, Y., Liu, G., Zuo, S., Ji, Y., Lu, A., Nakamura, M., Lazarus, M., Stratakis, C.A., Breyer, R.M., and Yu, Y. (2016). PKA regulatory IIα subunit is essential for PGD2-mediated resolution of inflammation. J. Exp. Med. *213*, 2209–2226. https://doi.org/10.1084/jem.20160459.

Korotkevich, G., Sukhow, V., and Sergushchev, A. (2019). Fast gene set enrichment analysis. Preprint at bioRxiv. https://doi.org/10.1101/060012.

Krämer, A., Green, J., Pollard, J., and Tugendreich, S. (2014). Causal analysis approaches in ingenuity pathway analysis. Bioinformatics *30*, 523–530. https://doi.org/10.1093/bioinformatics/btt703.

Lazear, H.M., Lancaster, A., Wilkins, C., Suthar, M.S., Huang, A., Vick, S.C., Clepper, L., Thackray, L., Brassil, M.M., Virgin, H.W., et al. (2013). IRF-3, IRF-5, and IRF-7 coordinately regulate the type I IFN response in myeloid dendritic cells downstream of MAVS signaling. PLoS Pathog. *9*, e1003118. https://doi.org/10.1371/journal.ppat.1003118.

Li, C., Zhang, Y., Liu, J., Kang, R., Klionsky, D.G., and Tang, D. (2021). Mitochondrial DNA stress triggers autophagy-dependent ferroptotic death. Autophagy *17*, 948–960. https://doi.org/10.1080/15548627.2020.1739447.

Liao, C., Rikke, B.A., Johnson, T.E., Diaz, V., and Nelson, J.F. (2010). Genetic variation in the murine lifespan response to dietary restriction: from life extension to life shortening. Aging Cell *9*, 92–95. https://doi.org/10.1111/j.1474-9726.2009.00533.x.

Liu, K., Liu, B., and Heilbronn, L.K. (2020). Intermittent fasting: what questions should we be asking? Physiol. Behav. *218*, 112827. https://doi.org/10.1016/j.physbeh.2020.112827.

Longo, V.D., and Panda, S. (2016). Fasting, circadian rhythms, and time-restricted feeding in healthy lifespan. Cell Metab. *23*, 1048–1059. https://doi.org/10.1016/j.cmet.2016.06.001.

Longo, V.D., and Cortellino, S. (2020). Fasting, dietary restriction, and immunosenescence. J. Allergy Clin. Immunol. *146*, 1002–1004. https://doi.org/10.1016/j.jaci.2020.07.035.

Lopez-Otin, C., Blasco, M.A., Partridge, L., Serrano, M., and Kroemer, G. (2013). The hallmarks of aging. Cell *153*, 1194–1217. https://doi.org/10.1016/j.cell.2013.05.039.

Love, M., Huber, W., and Anders, S. (2014). Differential analysis of count data–the DESeq2 package. Genome Biol. *15*. https://doi.org/10.1186/s13059-014-0550-8.

Lu, J., Krepelova, A., Rasa, S.M.M., Annunziata, F., Husak, O., Adam, L., Nunna, S., and Neri, F. (2021). Characterization of an in vitro 3D intestinal organoid model by using massive RNAseq-based transcriptome profiling. Sci. Rep. *11*, 16668. https://doi.org/10.1038/s41598-021-96321-8.

Ma, S., Sun, S., Geng, L., Song, M., Wang, W., Ye, Y., Ji, Q., Zou, Z., Wang, S., He, X., et al. (2020). Caloric restriction reprograms the Single-Cell transcriptional landscape of rattus norvegicus aging. Cell *180*, 984–1001.e22. https://doi.org/10.1016/j.cell.2020.02.008.

Mana, M.D., Yin-Sheun Kuo, E., and Yilmaz, O.H. (2017). Dietary regulation of adult stem cells. Curr. Stem Cell Rep. *3*, 1–8. https://doi.org/10.1007/s40778-017-0072-x.

Mazgaeen, L., and Gurung, P. (2020). Recent advances in lipopolysaccharide recognition systems. Int. J. Mol. Sci. *21*, 379. https://doi.org/10.3390/ijms21020379.

Mercken, E.M., Crosby, S.D., Lamming, D.W., JeBailey, L., Walker, S.K., Villareal, D.T., Capri, M., Franceschi, C., Zhang, Y., Becker, K., et al. (2013). Calorie restriction in humans inhibits the PI 3 K/AKT pathway and induces a younger transcription profile. Aging Cell *12*, 645–651. https://doi.org/10.1111/acel.12088.

Meydani, S.N., Das, S.K., Pieper, C.F., Lewis, M.R., Klein, S., Dixit, V.D., Gupta, A.K., Villareal, D.T., Bhapkar, M., Huang, M., et al. (2016). Long-term moderate calorie restriction inhibits inflammation without impairing cell-mediated immunity: a randomized controlled trial in non-obese humans. Aging (Albany NY) *8*, 1416–1431. https://doi.org/10.18632/aging.100994.

Moyse, E., Bèdard, K., Segura, S., Mahaut, S., Tardivel, C., Ferland, G., Lebrun, B., and Gaudreau, P. (2012). Effects of aging and caloric restriction on brainstem satiety center signals in rats. Mech. Ageing Dev. *133*, 83–91. https://doi.org/10.1016/j.mad.2012.01.004.

Nencioni, A., Caffa, I., Cortellino, S., and Longo, V.D. (2018). Fasting and cancer: molecular mechanisms and clinical application. Nat. Rev. Cancer *18*, 707–719. https://doi.org/10.1038/s41568-018-0061-0.

Nunna, S., Huang, Y.-P., Rasa, M., Krepelova, A., Annunziata, F., Adam, L., Käppel, S., Hsu, M.-H., and Neri, F. (2021). Characterization of novel alpha-Mangostin and Paeonol derivatives with cancer-selective cytotoxicity. Mol. Cancer Ther. *21*, 257–270. https://doi.org/10.1158/1535-7163.MCT-20-0787.

Oldenburg, M., Krüger, A., Ferstl, R., Kaufmann, A., Nees, G., Sigmund, A., Bathke, B., Lauterbach, H., Suter, M., Dreher, S., et al. (2012). TLR13 recognizes bacterial 23S rRNA devoid of erythromycin resistance–forming modification. Science *337*, 1111–1115. https://doi.org/10.1126/science.1220363.

Pan, F., Zhang, L., Li, M., Hu, Y., Zeng, B., Yuan, H., Zhao, L., and Zhang, C. (2018). Predominant gut Lactobacillus murinus strain mediates anti-inflammaging effects in calorie-restricted mice. Microbiome *6*, 1–17. https://doi.org/10.1186/s40168-018-0440-5.

Picelli, S., Bjorklund, A.K., Reinius, B., Sagasser, S., Winberg, G., and Sandberg, R. (2014). Tn5 transposase and tagmentation procedures for massively scaled sequencing projects. Genome Res. *24*, 2033–2040. https://doi.org/10.1101/gr.177881.114.

Ramana, C.V., Chatterjee-Kishore, M., Nguyen, H., and Stark, R.G. (2000). Complex roles of Stat1 in regulating gene expression. Oncogene *19*, 2619–2627. https://doi.org/10.1038/sj.onc.1203525.

Rivieccio, M.A., John, G.R., Song, X., Suh, H.S., Zhao, Y., Lee, S.C., and Brosnan, F. (2005). The cytokine IL-1β activates IFN response factor 3 in human fetal astrocytes in culture. J. Immunol. *174*, 3719–3726. https://doi.org/10.4049/jimmunol.174.6.3719.

Robertson, L.T., and Mitchell, J.R. (2013). Benefits of short-term dietary restriction in mammals. Exp. Gerontol. *48*, 1043–1048. https://doi.org/10.1016/j.exger.2013.01.009.

Salminen, A., Huuskonen, J., Ojala, J., Kauppinen, A., Kaarniranta, K., and Suuronen, T. (2008). Activation of innate immunity system during aging: NF-kB signaling is the molecular culprit of inflamm-aging. Ageing Res. Rev. *7*, 83–105. https://doi.org/10.1016/j.arr.2007.09.002.

Salminen, A., Kaarniranta, K., and Kauppinen, A. (2012). Inflammaging: disturbed interplay between autophagy and inflammasome. Aging (AlbanyNY) *4*, 166–175. https://doi.org/10.18632/aging.100444.

Sivo, J., Harmon, J.M., and Vogel, S.N. (1996). Heat shock mimics glucocorticoid effects on IFN-gamma-induced Fc gamma RI and Ia messenger RNA expression in mouse peritoneal macrophages. J. Immunol. *156*, 3450–3454.

Spaulding, C.C., Walford, R.L., and Effros. (1997). Calorie restriction inhibits the age-related dysregulation of the cytokines TNF-alpha and IL-6 in C3B10RF1 mice. Mech Ageing Dev *93*, 87–94. https://doi.org/10.1016/s0047-6374(96)01824-6.

Thevaranjan, N., Puchta, A., Schultz, C., Naidoo, A., Szamosi, J.C., Verschoor, C.P., Loukov, S., Schenck, L.P., Jury, J., Foley, K.P., et al. (2017). Age-associated microbial dysbiosis promotes intestinal permeability, systemic inflammation, and macrophage dysfunction. Cell Host Microbe *21*, 455–466.e454. https://doi.org/10.1016/j.chom.2017.03.002.

Trapnell, C., Roberts, A., Goff, L., Pertea, G., Kim, D., Kelley, D.R., Pimentel, H., Salzberg, S.L., Rinn, J.L., and Pachter, L. (2012). Differential gene and transcript expression analysis of RNA-seq experiments with TopHat and Cufflinks. Nat. Protoc. *7*, 562–578. https://doi.org/10.1038/nprot.2012.016.

Vanamee, É.S., and Faustman, D.L. (2018). Structural principles of tumor necrosis factor superfamily signaling. Sci. Signal. *11*, eaao4910. https://doi.org/10.1126/scisignal.aao4910.

Xia, S., Zhang, X., Zheng, S., Khanabdali, R., Kalionis, B., Wu, J., Wan, W., and Tai, X. (2016). An update on inflammaging: mechanisms, prevention, and treatment. J. Immunol. Res. *2016*, 8426874. https://doi.org/10.1155/2016/8426874.

Xie, J., Zhang, X., and Zhang, L. (2013). Negative regulation of inflammation by SIRT1. Pharmacol. Res. *67*, 60–67. https://doi.org/10.1016/j.phrs.2012.10.010.

Xu, L., Zhou, X., Wang, W., Wang, Y., Yin, Y., van der Laan, L.J.W., Sprengers, D., Metselaar, H.J., Peppelenbosch, M.P., and Pan, Q. (2016). IFN regulatory factor 1 restricts hepatitis E virus replication by activating STAT1 to induce antiviral IFN-stimulated genes. FASEB J. *30*, 3352–3367. https://doi.org/10.1096/fj.201600356R.

Ye, J., and Keller, J.N. (2010). Regulation of energy metabolism by inflammation: a feedback response in obesity and calorie restriction. Aging (Albany NY) *2*, 361–368. https://doi.org/10.18632/aging.100155.

Yu, Q., Zou, L., Kong, Z., and Yang, L. (2020). Cognitive impact of calorie restriction: a narrative review. J. Am. Med. Dir. Assoc. *21*, 1394–1401. https://doi.org/10.1016/j.jamda.2020.05.047.

Zhang, Y., Liu, T., Meyer, C.A., Eeckhoute, J., Johnson, D.S., Bernstein, B.E., Nusbaum, C., Myers, R.M., Brown, M., Li, W., and Liu, X.S. (2008). Model-based analysis of ChIP-seq (MACS). Genome Biol. *9*, R137. https://doi.org/10.1186/gb-2008-9-9-r137.

Zhang, C., Li, S., Yang, L., Huang, P., Li, W., Wang, S., Zhao, G., Zhang, M., Pang, X., Yan, Z., et al. (2013). Structural modulation of gut microbiota in life-long calorie-restricted mice. Nat. Commun. *4*, 1–10. https://doi.org/10.1038/ncomms3163.

Zhang, Y., and Liu, Z. (2017). STAT1 in cancer: friend or foe? Discov. Med. *24*, 19–29.

STAR★METHODS

KEY RESOURCES TABLE

REAGENT or RESOURCE	SOURCE	IDENTIFIER
Critical Commercial Assays		
TruSeq™ RNA Library Preparation Kit v2 -Set A	Illumina	RS-122-2001
TruSeq™ RNA Library Preparation Kit v2 -Set B	Illumina	RS-122-2002
NextSeq® 500/550 High Output Kit v2.5	Illumina	20024906
Mouse IFN-γ ELISA Kit II	Biosciences	558258
iScript cDNA Synthesis Kit	Bio-Rad	1708891
Sybr GreenER	Invitrogen	11761
QIAzol Lysis Reagent	QIAGEN	79306
Mouse Interferon alpha 1 ELISA Kit	Abcam	ab252352
ToxinSensor™ LAL Endotoxin Assay Kit	GenScript	L00350
Mouse IFN beta ELISA Kit	Abcam	ab252363
DMEM high glucose GlutaMAX pyruvate	Life Technologies	31966–021
Penicillin-Streptomycin	Life Technologies	15140-122
Fetal Bovine Serum	Life Technologies	26010066
Collagenase D	Roche (Sigma)	1108866001
DNaseI	Sigma	DN25
RBC lysis buffer	Cell Signaling Technology	46232
Pierce BCA Protein Assay Kit	Thermo Fisher Scientific	23225
Tn5 transposase	this manuscript	
y-27632 dihydrochloride	Sigma	Y0503
Antibodies		
FITC-conjugated anti-mouse CD45	BioLegend	Cat# 103107; RRID: AB_312972
Brillant Violet 605 anti-mouse CD45	BioLegend	Cat# 103139; RRID: RRID:AB_2562341
Sirt1 antibody	Cell Signaling	Cat# 2028S; RRID: AB_1196631
Anti-IRF3 antibody	Abcam	Cat# ab68481; RRID: AB_11155653
Stat1 antibody	Cell Signaling	Cat# 9172S; RRID: AB_2198300
Anti-TLR4 antibody	Abcam	Cat# ab13556; RRID: AB_300457
Deposited data		
RNA-seq; ATAC-seq	GeoDatasets	GSE162803
Scripts and Supplemental files	GitHub	https://github.com/smmrasa/DR_ATAC-seq_RNA-seq.git
Experimental models: Organisms/strains		
C57BL/6J	Jackson Lab	Stock: 000664
Oligonucleotides		
primers sequences can be found in Table S4		
Software and algorithms		
Prism software 7.0c	GraphPad	RRID: SCR_002798
RStudio v1.1.4	RStudio, Inc	RRID:SCR_000432
R v3.6.3	R Project	SCR_001905
Ingenuity Pathway Analysis (IPA)	QIAGEN	RRID:SCR_008653
FastQC v0.11.5	Babraham Bioinformatics, UK	RRID:SCR_014583
DESeq2 v1.20.0	Love et al. (2014)	RRID:SCR_015687
TopHat v2.1.0	Trapnell et al. (2012)	RRID:SCR_013035

(*Continued on next page*)

Continued

REAGENT or RESOURCE	SOURCE	IDENTIFIER
HTSeq-Count v0.11.2	Anders et al., (2015)	RRID:SCR_011867
Fgsea v1.10.1	Korotkevich et al. (2019)	RRID:SCR_020938
FASTX Toolkit v0.0.13	Hannon Lab, CSHL, USA	RRID:SCR_005534
MACS v1.4.2	Zhang et al. (2008)	RRID:SCR_013291
TCseq v1.2.0	Broad Institute, USA	N/A
Mixtools v1.2.0	Benaglia et al. (2009)	N/A
Homer v4.9.1	Heinz et al. (2010)	RRID:SCR_010881

RESOURCE AVAILABILITY

Lead contact

Prof. Francesco Neri francesco.neri@leibniz-fli.de. Current address: francesco.neri@unito.it.

Materials availability

Any materials generated in this study are being made available. Further information and requests for resources and reagents should be directed to the lead contact.

Data and code availability

- Sequencing data and codes used in this study are fully available.
- Sequencing data have been deposited on GeoDatasets under the Geo Accession Code: GSE162803. The codes, the scripts and supplemental files are deposited in GitHub: https://github.com/smmrasa/DR_ATAC-seq_RNA-seq.git.
- Any additional information required to reanalyze the data reported in this paper is available from the lead contact upon request

EXPERIMENTAL MODEL AND SUBJECT DETAILS

Mice

All wild-type mice were C57BL/6J obtained from Janvier Labs. All animals were kept in a specific pathogen-free animal facility with a 12 h light/dark cycle. Dietary restriction experiments were performed on female mice. Young mice were aged 4 months, old mice were aged 24 months. For each condition we used a mouse number ≥ 4.

METHOD DETAILS

Dietary restriction

One week before dietary restriction feeding, the animals were separated to single cages. Food weight and body weight were measured directly after separating the animals and before the dietary treatment starting. The daily food intake per animal was calculated and used for calculating the amount that refers to 70% for every animal dependent on its body weight. Food (ssniff #V1524-786) was given during the morning once per day to the DR animals. The AL animals had unlimited access to food during all the experimental time. As usual and unavoidable in calorie-restriction experiments, the calorie-restricted mice usually consume their food in $\sim$6 h, and result in having daily fasting period of $\sim$18 h. Both DR and AL animals had unlimited access to the water.

Sample collection

Mice were sacrificed by CO_2 inhalation and exsanguinated. Whole organs were extracted and cut into 2–4 pieces, respectively (100–300 mg/piece). Each sample was then quickly frozen in liquid nitrogen and stored at -80°C until nuclei extraction was performed. In this study, we used 8 different organs or tissues: blood, brain, heart, kidney, liver, lung, muscle and skin. For each condition we used a mouse number ≥ 4.

Mouse serum collection

Mice were sacrificed by CO_2 inhalation. Immediately after, the blood was drawn directly from the heart, with a needle 26G. The blood was then left at RT for 30 min at RT, to let the corpuscular part coagulates. After that, the samples were centrifuged for 15 min at 4°C at 1200g for the serum collection. Serum was then immediately used or stored in the -20°C. For each condition we used a mouse number ≥ 4.

ELISA detection

Measurement of the concentration of Ifng, Ifna, Ifnb and endotoxin was performed by using ELISA kits (see STAR Methods) by following the manufacturer's protocol. The sample's concentrations were derived by using the derived standard curve slope. For each condition we used a mouse number ≥ 4.

Flow cytometry

For the preparation of the single cell suspension from kidney, liver, and lung, the tissues were first mechanically disrupted by cutting them into 0.5 mm^3 pieces with the help of a fine scalpel and then enzymatically digested for 45 min at 37°C on a shaker with Collagenase D (0.125 mg/mL, Roche (Sigma)) and DNase I (0.1 mg/mL, Sigma) in DMEM high glucose GlutaMAX pyruvate (Life technologies), supplemented with 1% fetal bovine serum (FBS) (Life technologies), 1% Penicillin-Streptomycin (Pen/Strep) (Life technologies). Single cell suspensions were filtered through a 70 μm cell strainer to remove any residual undigested tissue. Erythrocytes were removed by using red blood cell (RBC) lysis buffer (Cell Signaling Technology). Single cell suspensions were incubated with a fluorescein isothiocyanate- (FITC) conjugated anti-mouse CD45 (BioLegend) antibody or with a Brillant Violet- (BV) 605 anti-mouse CD45 (BioLegend) antibody for 30–60 min at 4°C in PBS supplemented with 2% FBS and 10 μM ROCK inhibitor y-27632 dihydrochloride (Sigma). The CD45 positive (+) and CD45 negative (−) cells were analyzed and sorted with FACS Aria (BD Biosciences) after excluding residual erythrocytes, debris, doublets and dead cells by forward scatter (FSC), side scatter (SSC) and 4′, 6-Diamidino-2-phenylindole dihydrochloride (DAPI) gating.

Total RNA sequencing library preparation

RNA was isolated, quantified and quality assessed as previously described (Lu et al., 2021) by using the Standard Sensitivity RNA analysis Kit; 15nt DNF-471-0500 (Advanced Analytical). Samples with degraded RNA were excluded for further analysis. RNA samples were further processed for Total RNA-seq library preparation according to the manufacturer's instructions (TruSeq^{R}RNA Sample preparation v2, Illumina). For each condition we used a mouse number ≥ 4. See Table S3.

Reverse transcription and real-time qPCR

iScript cDNA Synthesis Kit (Bio-Rad Laboratories GmbH 1708891) was used for cDNA synthesis starting from RNA according to the manufacture's protocol. Relative gene expression analysis was done using quantitative real-time PCR software. The expression levels of target genes were normalized to that of the housekeeping gene (Gapdh). Statistical analysis was made using GraphPad Prism software 7.0c. Unpaired t test was used to calculate the significance and p value <0.05 was considered significant. Shapiro Wilk test was used to calculate the normality before to apply the test. For each condition n (biological replicates) ≥ 3.

Western Blot

Liver and kidney tissues were incubated with RIPA buffer on ice for 15 min and sonicated using the BioruptorPico (Diagenode) for five cycles. After cold centrifugation at 20,000g for15 min, the supernatant was collected and the total protein concentration was measured using Pierce BCA Protein Assay Kit (Thermo Fisher Scientific). Western blots were performed as previously described with over-night primary antibodies incubation (Nunna et al., 2021).

Preparation of recombinant Tn5 transposase

The pTXB1-Tn5 plasmid was a gift from Rickard Sandberg (Addgene plasmid #60240). The gene encoding Tn5 was further mutated to introduce the R27S mutation described by Hennig et al. (2018). The hyperactive Tn5 protein was expressed and purified similarly as described (Picelli et al., 2014) with minor modifications. The Tn5 protein was expressed in BL21 (DE3) Codonplus RIL cells. For this, two liters of Terrific Broth supplemented with ampicillin was inoculated with freshly transformed pTXB1-Tn5 R27S colonies. The inoculated culture was grown at 37°C in a shaking incubator until OD600 of 0.6. Subsequently, the flasks were then chilled on ice for ~20 min and the protein expression was induced with 1 mM IPTG. The culture was further grown at 23°C for 4–5 h and the cells were harvested by centrifugation, washed with 1x STE buffer and stored at −20°C. For purification, the cell pellets were resuspended in 160 mL of lysis buffer (20 mM HEPES-KOH, pH 7.2, 0.8 M NaCl, 1 mM EDTA, 10% glycerol, 0.2% Triton X-100) and the cells were disrupted by sonication on a Branson sonicator. Crude extract was cleared by centrifugation and the cleared lysate was further depleted of DNA/RNA by dropwise addition of 4.2 mL of 10% neutralized PEI. The formed precipitate was removed by centrifugation at 12,000 rpm for 10 min at 4°C. Subsequently, the supernatant was loaded onto a gravity-flow column packed with 2 mL of chitin beads (S6651S, NEB) and washed with 300 mL of the lysis buffer. The Tn5 protein was eluted by cleavage of the intein with 100 mM DTT supplemented in the lysis buffer for 36 h at 4°C. 1 mL elution fractions were collected and the most concentrated fractions were pooled and dialyzed against 1 L of dialysis buffer (100 mM HEPES-KOH, pH 7.2, 0.2 M NaCl, 0.2 mM EDTA, 2 mM DTT, 0.2% Triton X-100, 50% glycerol). The concentration of the dialyzed protein was measured with Nanodrop and the purified protein was stored at −20°C until further use.

ATAC-seq library preparation

10–30 mg of tissues were homogenized in a 2 mL Eppendorf tubes (with a tight pestle) with 15 strokes in 0.5 mL of liquid nitrogen on dry ice. Pulverized tissues were then suspended in cold 1X PBS, centrifuged at 2000 g × 3 min at 4 C. After centrifugation, the

supernatants were removed and the pellets were resuspended in tissue lysis buffer (with anti-protease). Tubes were rocked for 10 min at 4 C and then transferred to a glass douncer and homogenized with 15 strokes. After centrifuged at 800 g × 5 min at 4 C, nuclei were resuspended in PBS, filtered with a 40 μm cell strainer and stained with Trypan blue and then counted. Approximately 50000 nuclei were transferred into a fresh tube and in 50 μL transposition reaction mixture containing 50 mM TAPS-NaOH (pH 8.5), 25 mM $MgCl_2$, 50% DMF, 5 μL of Tn5 transposase, for 60 mins at 37°C. Afterward, the DNA was purified with MinElute Purification Kit (Qiagen) and amplified with primers containing barcodes, as previously described (Picelli et al., 2014). For each condition we used a mouse number ≥4 (see Table S3).

QUANTIFICATION AND STATISTICAL ANALYSIS

RNA-seq data analysis

Quality control and mapping

Fastq files quality check was performed using FastQC v0.11.5. The fastq files were mapped to the mm9 (NCBI37) genome using TopHat v2.1.0 (Trapnell et al., 2012) with the following parameters –bowtie1 –no-coverage-search -a 5.

Differentially expression analysis

The number of reads covered by each gene was calculated by HTSeq-Count 0.11.2 (Anders et al., 2015) with -s no -a 0 -t exon -m intersection-nonempty parameters (NCBI37 RefSeq Gene annotation). Before further analysis, all of the rRNA genes were removed from the count data. The FPKM (Fragment per kilo base pair transcript per million sequenced reads) was calculated using the HTSeq counts and a custom script. For calculating differentially expressed genes and normalized count, DESeq2 R package v1.20.0 (Love et al., 2014) was used with the default parameters.

Principal component analysis (PCA)

For PCA plot (Figures 1B–1D), the normalized count was used and the genes were filtered using the following criteria, count>10 in at least 3 samples, IQR of the log transform count ≥ mean of the IQR of log transformed count in all genes. After filtering, the log 10 transformed count was used in prcomp R function with center = TRUE, scale. = TRUE parameters. PC1 and PC2 were used for the plotting. To calculate the rescue of the DR samples (Figure 1E), the average of PC1 and PC2 of all of the replicates for each group were used as a representative for each group. To make the calculations easier, the PCA plot (PC1 and PC2) was converted to polar coordinate system with the center of the young group as the reference (zero) point (by subtracting the PC1 and PC2 of each point form the young). The following calculation was done on the polar coordinate system with young as 0,0 point. The distance between young and old were calculated by $l_{\mathrm{Old}} = \sqrt{pc1_{old}{}^2 + pc2_{old}{}^2}$ formula. With a similar formula, the distance between LTDR(l_{LTDR}) and STDR(l_{STDR}) to the young was also calculated. To calculated the length of the perpendicular line connecting LTDR and STDR to the aging line (the line connects the young and old) the following calculations were done. The angle of the LTDR and STDR ($\alpha_{DR(LTorST)}$) to the reference point (young) was calculated using $\alpha_{DR(LT\ or\ ST)} = \tan^{-1}\frac{pc2_{DR(LT\ or\ ST)}}{pc1_{DR(LT\ or\ ST)}} - \tan^{-1}\frac{pc2_{Old}}{pc1_{Old}}$ formula and the length of the perpendicular line connecting LTDR and STDR to the aging line ($\mathrm{LPA_{LTDR}}$ and $\mathrm{LPA_{STDR}}$) was calculated by $LPA_{DR(LTor\ ST)} = l_{DR(LT\ or\ ST)} \times \sin \alpha_{DR(LT\ or\ ST)}$ formula. To calculate the rescue ($\mathrm{R_{STDR}}$ and $\mathrm{R_{LTDR}}$), $R_{DR(LTor\ ST)} = \sqrt{l_{DR(STorLT)}{}^2 - \mathrm{LPA_{DR(LT\ or\ ST)}}^2}$ and the normalized percentage of rescue $NR_{DR(LT\ or\ LT)} = \left(1 - \frac{R_{DR(LTorST)}}{l_{Old}}\right) \times 100$ formulas were used (Figure S1B).

Pathway and upstream regulators analysis

For functional and pathway analysis as well as upstream regulators analysis, IPA (Ingenuity Pathway Analysis v45868156) software has been used (Krämer et al., 2014) with DEG (padj<0.05).

To find the top common upstream regulators (Figure 3A), DESeq2 differentially expression analysis (padj<0.05) results of all of the 24 comparisons (8 tissues, 3 conditions: young versus old, old versus LTDR, old versus STDR) were uploaded in IPA. Out of 1500 upstream regulators, just those which their predicted activity significantly changed (|*Z* score|>2) at least in 12 conditions have been selected for the downstream analysis. In addition, only the upstream regulators relating to the immune system regulation and inflammation were further selected. All of the known direct target genes for each selected upstream regulator (only transcriptional regulation) as well as the known direction of the regulation (activation or inhibition) were extracted from IPA.

For Gene Set Enrichment Analysis (GSEA), to exclude the not expressed genes for each tissue and condition, the gene set was filtered on the base mean calculated by the DESeq2 (base mean>=5). The log2 fold change (DESeq2) for each gene was multiplied by the direction (+1 for the activation and −1 for the inhabitation) and used for the ranking of the genes. The ranked gene list was used in the fgsea function in the fgsea_1.10.1 R package (Korotkevich et al., 2019) with nperm = 10000. Calculated normalized enrichment score (NES) and p value was used for the plotting. The target genes direction was extracted from the IPA.

For constructing the network (Figures 3C and S2), the known direct connections (only transcriptional regulation) between the selected upstream regulators were extracted from IPA. The upstream regulators which were not connected (or has few connections) to this network has been removed. In addition, the regulators with very similar gene target (more than 70%) were removed from the network. Three extra upstream regulators have been added to the network, the LPS which is a chemical upstream regulator (LPS passed the filter of activity prediction in 17 condition), the Sirt1 and Cebpb which are the known key player in DR and gives us a hint to connect the metabolism to the inflammation. The network was plotted with igraph_1.2.4.1 R package. Each node in the graph

(upstream regulators) is a pie chart and the size of the node represents the sum of -log10 of enrichment p value for all of the tissues showed as the color of the pie chart. The tissue with non-significant enrichment (p value<0.05) or enriched in the opposite direction of the other tissues (the direction is mentioned below the title of each upstream regulator) were removed from the plot and the calculations. Each slice in the pie chart represents the -log10 enrichment p value of the corresponding tissue.

The gene set used for Figure 4B has been extracted from IPA by selecting all of the differentially expressed genes in different tissues/conditions which were categorized as inflammatory response in IPA disease and function section. In addition, the direction of the genes (activated or inhibited) was extracted from IPA and used in GSEA analysis.

ATAC-seq data analysis

Quality check and mapping

Fastq files quality check was performed with FastQC (v0.11.5). The adopter sequence was removed using fastx_clipper (FASTX Toolkit 0.0.13) with the -a CTGTCTCTTATACACATCTGACGCTGCCGACGA -Q33 -l 20 -n -v -M 10 parameters. Fastq files mapping to mm9 (NCBI37) genome was performed using Bowtie (v1.1.2) with –best –strata -m 1 parameters. Duplicate reads were removed using a custom script. For peak calling, macs14 (v1.4.2) was used with –nolambda parameter and p value cutoffs of 10–5. For RPM (Read Per Milion) calculation (used for PCA analysis, Figure 6A), peaks (from macs) were merged using Peakreference function (TCseq_1.2.0 package). The merged peaks have been used as the reference for calculation of RPM for each sample by using a custom script. For FPKM (Fragment Per Kilobase pair region per Million sequenced reads), the RPM is normalized to the size of the studied region).

Open chromatin distribution analysis

The number and the distribution of peaks and reads covering the gene annotation (TSS and TES) were calculated using a custom script (Figures 6C, S5A and S5B).

For promoter analysis (Figures 6D, 6F, 6G, S5C, S5E, and S5F), the RPM/FPKM was calculated on the promoter of the longest isoform of each gene (± 1kb of TSS) using a custom script. The modeling of the open chromatin distribution on the promoter, was done using normalmixEM function in mixtools_1.2.0 R package with default parameters (Benaglia et al., 2009).

For plotting the promoter open chromatin versus expression (Figures 6H, 6I, S5G, and S5H), the genes which their expression were not changing have been removed (IQR>0) and the average of expression for each condition (young, old, LTDR), per gene has been calculated. The genes have been categorized into 20 groups based on the level of their expression in the young group using quantile function in R.

For plotting the FPKM of the peaks with Stat1, Irf7 and Irf3 motifs around the target genes of each transcription factor (Figures 7C, 7F,7I, S6C, S6F, and S6I), the merged reference peaks (p value<10-5) were used. The number of reads covering each peak were calculated using bedtools intersect (v2.28.0–33-g0f45761e). To remove the bias on the distribution of reads in promoter and gene body explained in the results, we selected only peaks with less than ±5kb to the TSS (longest isoform) for further analysis and as the reference for FPKM calculation. The peaks which were annotated to each transcription factor target genes (±5kb to the TSS) were searched for the binding motif using findMotifs.pl (homer-4.9.1). The motif sequence of STAT1.MA0137.3 (http://jaspar.genereg.net/matrix/MA0137.3/), PB0033.1_Irf3_1 (http://jaspar.genereg.net/matrix/PB0033.1_Irf3_1/), and IRF7.MA0772.1 (http://jaspar.genereg.net/matrix/MA0772.1/) has been used. The peaks which had at least 1 matched motif (score>=10) have been selected for plotting and p value calculation.

ADDITIONAL RESOURCES

Ethics statement

All animal experiments were carried out with the approval of the state government of Thuringia (license no. FLI-17-006).

Cell Reports, Volume *39*

Supplemental information

Inflammaging is driven by upregulation of innate immune receptors and systemic interferon signaling and is ameliorated by dietary restriction

Seyed Mohammad Mahdi Rasa, Francesco Annunziata, Anna Krepelova, Suneetha Nunna, Omid Omrani, Nadja Gebert, Lisa Adam, Sandra Käppel, Sven Höhn, Giacomo Donati, Tomasz Piotr Jurkowski, Karl Lenhard Rudolph, Alessandro Ori, and Francesco Neri

Supplemental Information

Supplemental Information contains 6 Supplemental Figures.

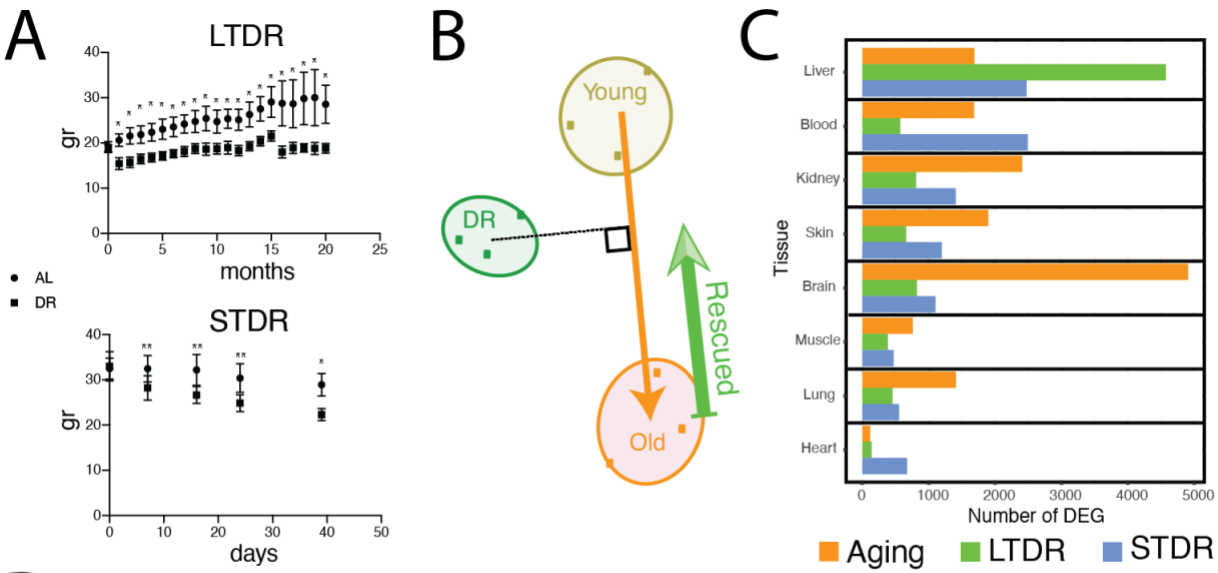

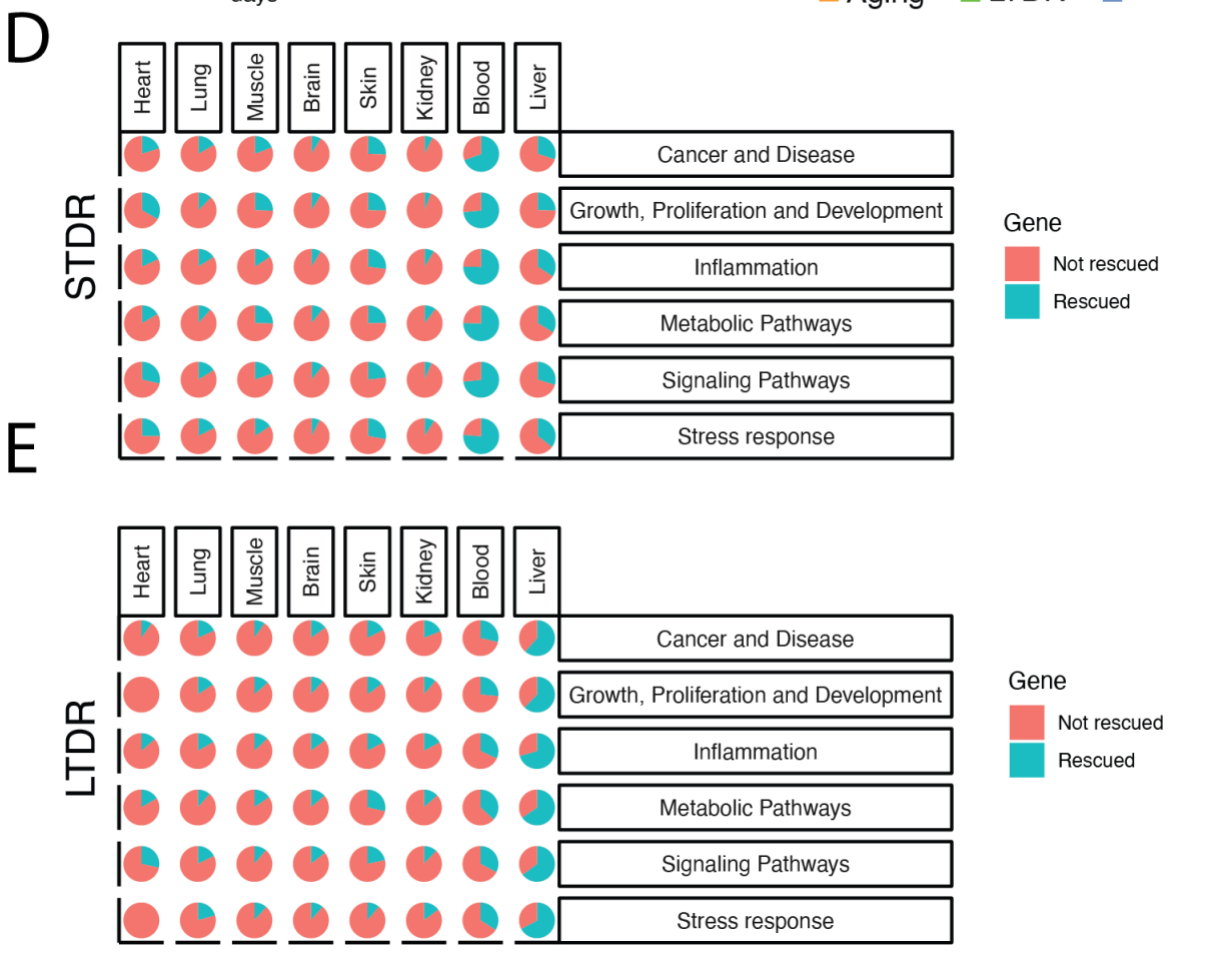

Figure S1. DR partially rescues aging transcriptome. Related to Figure 1.

A. Body weight curves of the LTDR and STDR mice compared with the control group of mice kept *ad libitum*. P-values are calculated with multiple t test, not assuming consistent SD and FDR approach. ** = $p<0.05$, * = $p<0.01$. Graphs show mean and SD.

B. The schematic picture explaining the calculation of the rescue from the PCA plot (Check the methods).

C. Number of differentially expressed genes (adjusted p-value<0.05). The Y axis shows the tissue and colors shows the conditions. For aging group, young is compared to the old, and for LTDR and STDR groups, the DR is compared to the old group.

D,E. Pie charts showing the percentage of rescued and not rescued genes by DR to the total number of DEGs related to each of the indicated functional category regulated by aging in the listed tissues.

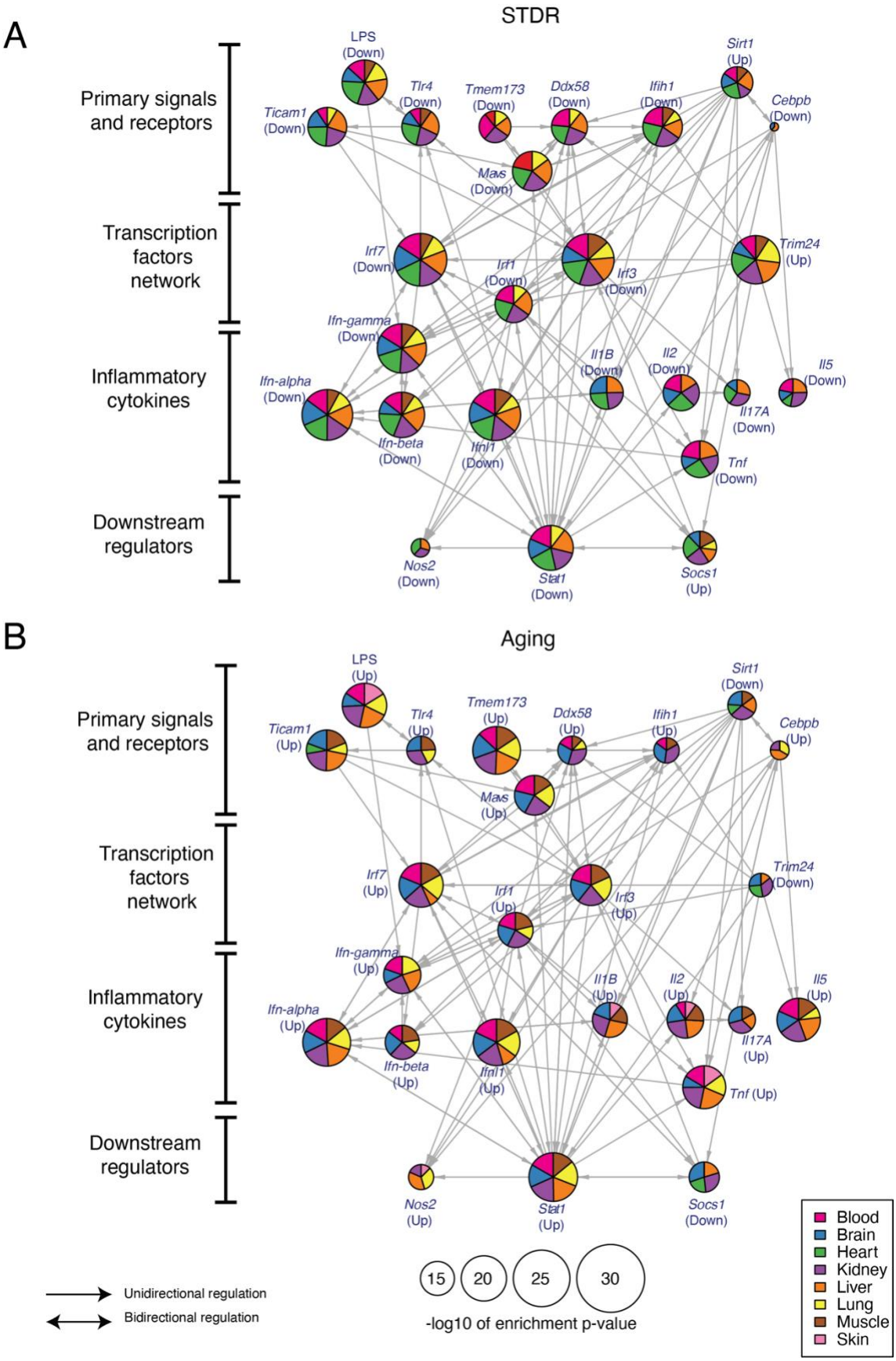
A
STDR
Primary signals and receptors
Transcription factors network
Inflammatory cytokines
Downstream regulators
LPS (Down)
Tlr4 (Down)
Tmem173 (Down)
Ddx58 (Down)
Ifih1 (Down)
Sirt1 (Up)
Cebpb (Down)
Ticam1 (Down)
Mavs (Down)
Irf7 (Down)
Irf1 (Down)
Irf3 (Down)
Trim24 (Up)
Ifn-gamma (Down)
Il1B (Down)
Il2 (Down)
Il5 (Down)
Ifn-alpha (Down)
Il17A (Down)
Ifn-beta (Down)
Ifnl1 (Down)
Tnf (Down)
Nos2 (Down)
Stat1 (Down)
Socs1 (Up)
B
Aging
Primary signals and receptors
Transcription factors network
Inflammatory cytokines
Downstream regulators
LPS (Up)
Tlr4 (Up)
Tmem173 (Up)
Ddx58 (Up)
Ifih1 (Up)
Sirt1 (Down)
Cebpb (Up)
Ticam1 (Up)
Mavs (Up)
Irf7 (Up)
Irf1 (Up)
Irf3 (Up)
Trim24 (Down)
Ifn-gamma (Up)
Il1B (Up)
Il2 (Up)
Il5 (Up)
Ifn-alpha (Up)
Il17A (Up)
Ifn-beta (Up)
Ifnl1 (Up)
Tnf (Up)
Nos2 (Up)
Stat1 (Up)
Socs1 (Down)
Unidirectional regulation
Bidirectional regulation
15
20
25
30
-log10 of enrichment p-value
Blood
Brain
Heart
Kidney
Liver
Lung
Muscle
Skin

Figure S2. The proposed network of upstream regulators regulating the inflammation in STDR(A) and aging(B). Related to Figure 3.

Each circle shows an upstream regulator. The size of the circle shows the sum of -log 10 of enrichment p-value for all of the tissues which are specified by the colors in each node. Each circle is a pie chart showing the contribution of different tissues in the sum of the -log10 p-values. Tissues with none-significant p-value (<0.05) or with opposite direction compared to the majority, has not been used in the pie chart and calculations. The parenthesis under the name of each upstream regulator shows the direction of the activity prediction.

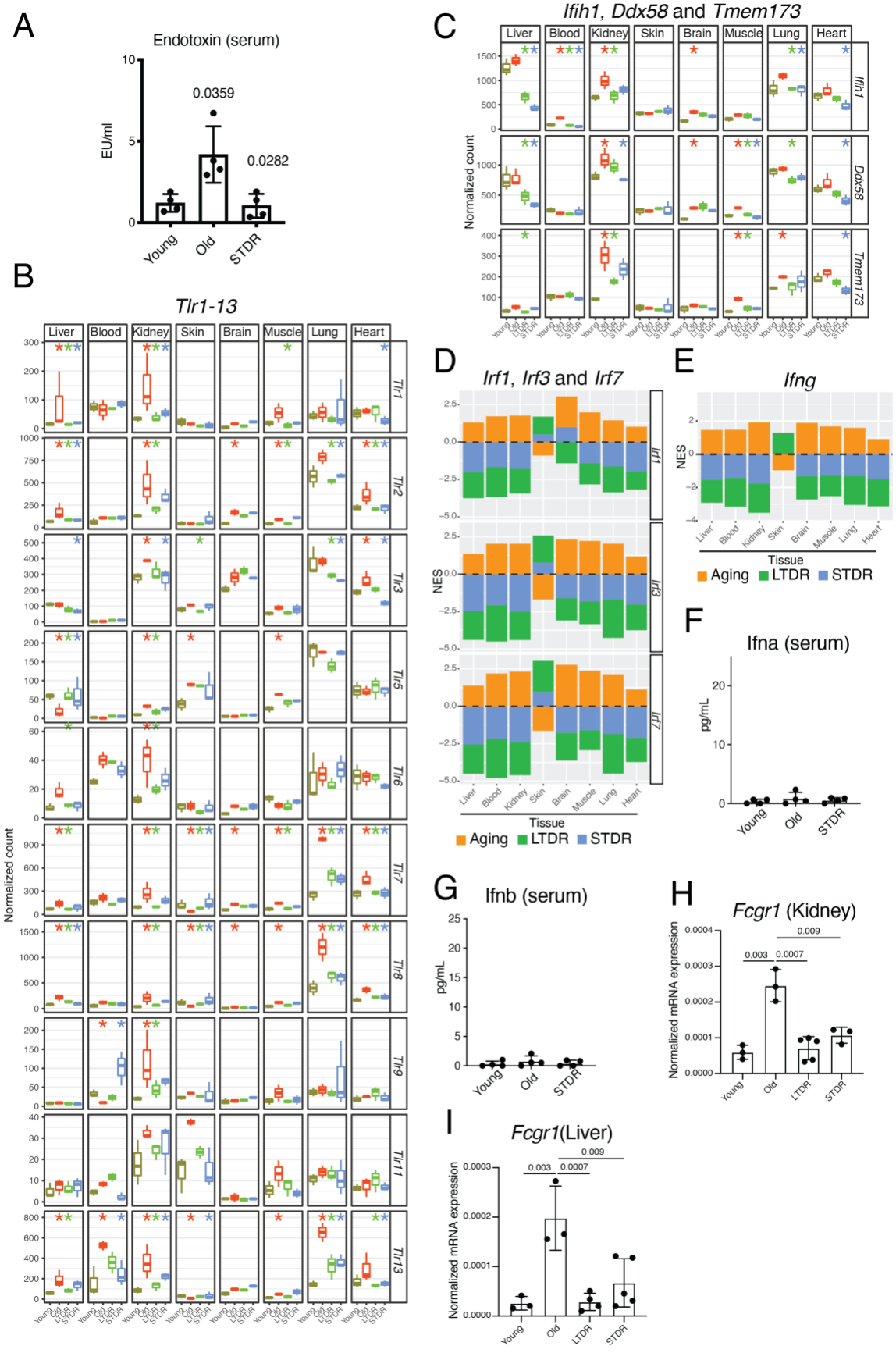
A
Endotoxin (serum)
EU/ml
0.0359
0.0282
Young
Old
STDR
B
Tlr1-13
Liver
Blood
Kidney
Skin
Brain
Muscle
Lung
Heart
Normalized count
Tlr1
Tlr2
Tlr3
Tlr5
Tlr6
Tlr7
Tlr8
Tlr9
Tlr11
Tlr13
C
Ifih1, Ddx58 and Tmem173
Ifih1
Ddx58
Tmem173
D
Irf1, Irf3 and Irf7
NES
Tissue
Aging
LTDR
STDR
E
Ifng
F
Ifna (serum)
pg/mL
G
Ifnb (serum)
H
Fcgr1 (Kidney)
Normalized mRNA expression
0.009
0.003
0.0007
I
Fcgr1(Liver)

Figure S3. DR rescues aging induced upregulation of innate immunity receptors and activation of interferon response. Related to Figure 4.

A. Bar chat indicating the level of endotoxin in the mouse blood serum measured by ELISA assay. P-value is calculated by 2-tailed unpaired Welch's t-test between Young and old as well as between Old and STDR. For each condition we used a mouse number = 4. Bar charts show mean ± SD.

B. Expression of *Tlr* gene family (*Tlr1-13*) in different tissues and conditions. P-value is calculated by DESeq2 comparing old with young and LTDR/STDR with old. *p-value<0.05

C. Expression of *Ifih1*, *Ddx58* and *Tmem173* in different tissues and conditions. P-value is calculated by DESeq2 comparing old with young and LTDR/STDR with old. *p-value<0.05

D. GSEA analysis for *Irf1*, *Irf3*, and *Irf7* in different tissues (X axis) and conditions(color). The Y axis shows normalized enrichment score (NES).

E. Interferon gamma (Ifng) activity predication (NES) based on the expression of its target genes. The condition which is not in the plot (STDR, skin) showed neither enrichment or depletion.

F and G. Bar chat indicating the level of Ifn-alpha and Ifn-beta in the mouse blood serum measured by ELISA assay. P-value is calculated by 2-tailed unpaired Welch's t-test between Young and old as well as between Old and STDR. No significant differences were observed. For each condition we used a mouse number = 4. Bar charts show mean ± SD.

H and I. *Fcgr1* (target of Ifng) expression in kidney (E) and Liver (F) measured by qRT-PCR. P-value is calculated by 2-tailed unpaired Welch's t-test. For each condition we used a mouse number ≥ 3. Bar charts show mean ± SD.

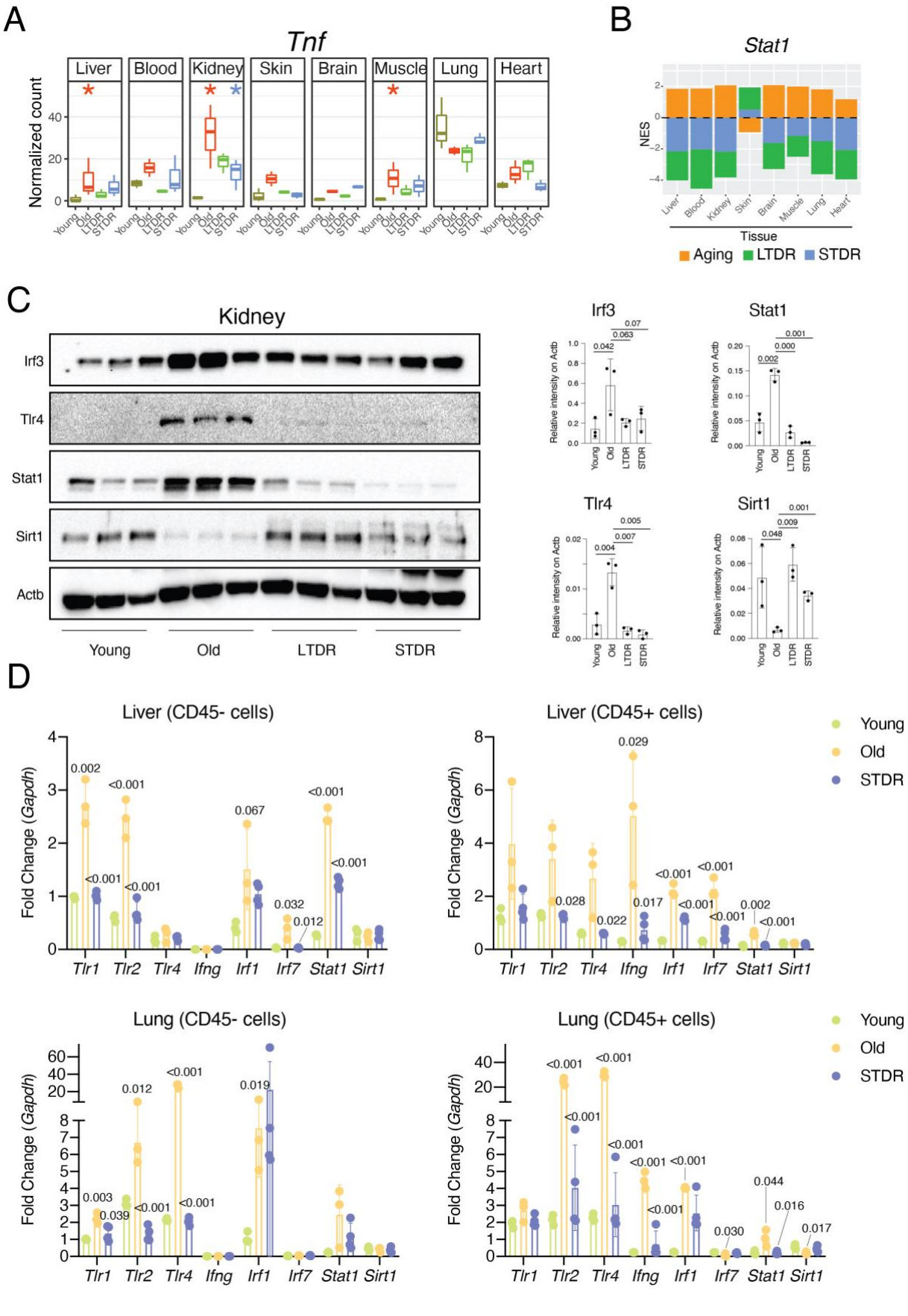
A
Tnf
Liver
Blood
Kidney
Skin
Brain
Muscle
Lung
Heart
Normalized count
Young
Old
LTDR
STDR
B
Stat1
NES
Tissue
Aging
LTDR
STDR
C
Kidney
Irf3
Tlr4
Stat1
Sirt1
Actb
Young
Old
LTDR
STDR
Relative intensity on Actb
D
Liver (CD45- cells)
Liver (CD45+ cells)
Lung (CD45- cells)
Lung (CD45+ cells)
Fold Change (Gapdh)
Tlr1
Tlr2
Tlr4
Ifng
Irf1
Irf7
Stat1
Sirt1

Figure S4. DR rescues aging induced upregulation of innate immunity receptors and activation of interferon response. Related to Figure 5.

A. *Tnf* expression in different tissues and conditions. P-value is calculated by DESeq2 comparing old with young and LTDR/STDR with old. *p-value<0.05

B. GSEA analysis for the expression of Stat1 target genes in different tissues (X axis) and conditions(color). The Y axis shows normalized enrichment score (NES).

C. Left panel: Western blotting of the indicated protein in the indicated tissue and conditions. Right panel: quantification of the western blot signals. Bar charts show mean ± SD. P-value is calculated by 1-tail Welch's t-test. For each condition we used a mouse number = 3.

D. Bar charts showing the results of the RT-qPCR of the indicated genes in CD45- and CD45+ cells in kidney. P-value is calculated by 2-tailed unpaired Welch's t-test between Young and old as well as between Old and STDR. Only significant comparisons (p-values < 0.05) are reported. For each condition we used a mouse number ≥ 3. Bar charts show mean ± SD.

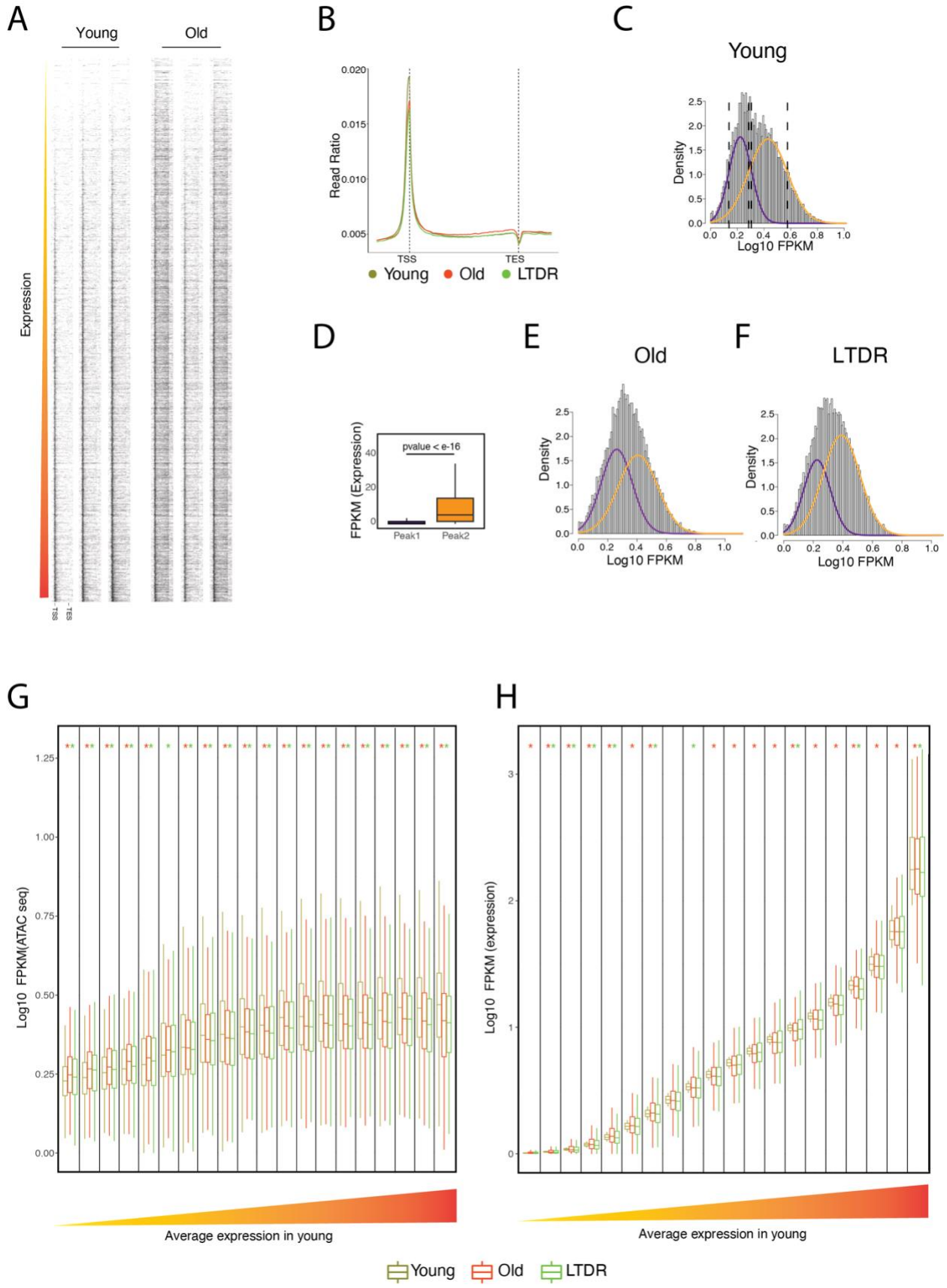
A
Young
Old
Expression
TSS
TES
B
Read Ratio
0.020
0.015
0.010
0.005
TSS
TES
Young
Old
LTDR
C
Young
Density
Log10 FPKM
D
FPKM (Expression)
pvalue < e-16
Peak1
Peak2
E
Old
Density
Log10 FPKM
F
LTDR
Density
Log10 FPKM
G
Log10 FPKM(ATAC seq)
Average expression in young
H
Log10 FPKM (expression)
Average expression in young
Young
Old
LTDR

Figure S5. Aging induced open chromatin re-arrangement results in transcriptional change depends on the basal level of gene expression. Related to Figure 6.

A. Heatmap shows the number of peaks (p-value < 10^{-5}) in respect to the gene annotation (TSS and TES) in young and old kidney samples. The genes are ordered from the low to the high expression in young group.

B. Relative sequenced read distribution (normalized to the total number of sequenced reads per sample) in respect to the gene annotation in liver. The dashed lines show the TSS (transcription start site) and the TES (transcription end site). Between the TSS and TES, the position (X axis) is relative to the gene size. Outside of the gene region (before TSS and after TES) the position are absolute. Average of the replicates for each group are used in the plotting.

C. The histogram shows the distribution of open chromatin of the promoter regions (±1kb of TSS of the longest isoform) in liver of the young group. Modeling of the distribution suggest two normal distributions. Mean ± standard deviation for each normal distribution is shown as dashed line.

D. The expression (FPKM) of genes representing each distribution (peak 1 and 2 represent the red and green distribution respectively in figure S4C) in liver. The p-value is calculated by 2-tailed Wilcoxon test.

E and F. Similar to C, the histogram shows the distribution of open chromatin of the promoter regions in liver of the old(E) and LTDR(F) group.

G. Box plot shows the open chromatin intensity (log10 FPKM of ATAC-seq data) in the promoter region of genes with different level of expression in liver. The genes are sorted based on their expression in the young group (X axis). P-value is calculated using 2-tailed paired t-test which the log10 FPKM (ATAC-seq) of each gene is compared in different groups. For p-value calculation, the old is compared to the young and the DRLT is compared to the old. *p-value<0.05.

H. Box plot shows the expression (log10 FPKM, Y axis) of the genes (liver) with different level of basal expression in young as figure S5G. P-value is calculated using 2-tailed paired t-test which the expression of each gene is compared in different groups. For p-value calculation, the old is compared to the young and the DRLT is compared to the old. *p-value<0.05.

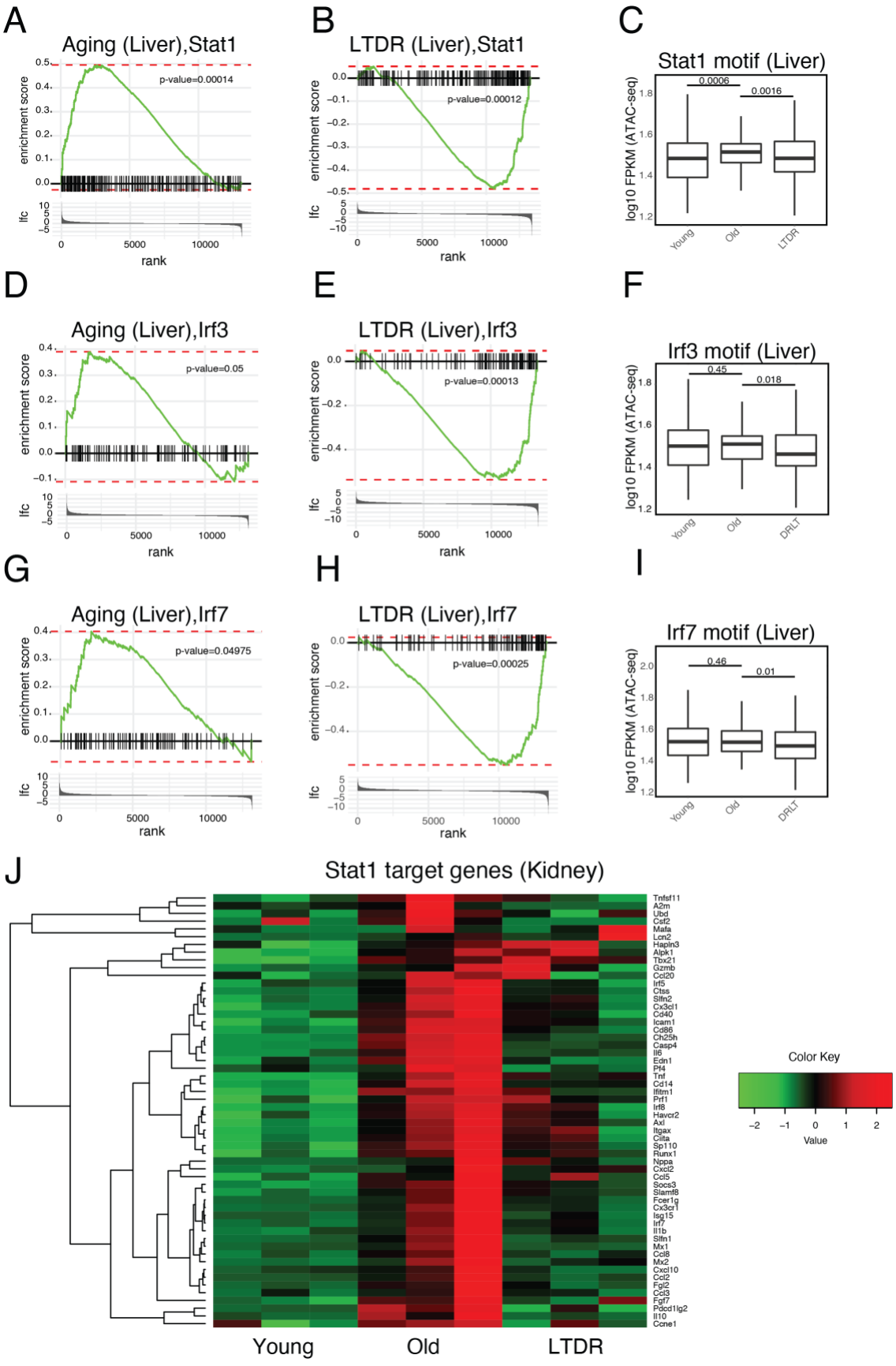
A
Aging (Liver),Stat1
p-value=0.00014
enrichment score
lfc
rank
B
LTDR (Liver),Stat1
p-value=0.00012
C
Stat1 motif (Liver)
0.0006
0.0016
log10 FPKM (ATAC-seq)
Young
Old
LTDR
D
Aging (Liver),Irf3
p-value=0.05
E
LTDR (Liver),Irf3
p-value=0.00013
F
Irf3 motif (Liver)
0.45
0.018
DRLT
G
Aging (Liver),Irf7
p-value=0.04975
H
LTDR (Liver),Irf7
p-value=0.00025
I
Irf7 motif (Liver)
0.46
0.01
J
Stat1 target genes (Kidney)
Tnfsf11
A2m
Ubd
Csf2
Mafa
Lcn2
Hapln3
Alpk1
Tbx21
Gzmb
Ccl20
Irf5
Ctss
Slfn2
Cx3cl1
Cd40
Icam1
Cd86
Ch25h
Casp4
Il6
Edn1
Pf4
Tnf
Cd14
Ifitm1
Prf1
Irf8
Havcr2
Axl
Itgax
Ciita
Sp110
Runx1
Nppa
Cxcl2
Ccl5
Socs3
Slamf8
Fcer1g
Cx3cr1
Isg15
Irf7
Il1b
Slfn1
Mx1
Ccl8
Mx2
Cxcl10
Ccl2
Fgl2
Ccl3
Fgf7
Pdcd1lg2
Il10
Ccne1
Color Key
Value
Young
Old
LTDR

Figure S6. ATAC-seq and RNA-seq data confirm the activation of Irf3,7 and Stat1 transcription factors in aging and inhibition by DR in liver. Related to Figure 7.

A and B: GSEA analysis of the Stat1 target genes expression in young versus old (A) and old versus LTDR (B) comparisons in liver. Stat1 target genes expression is positively enriched in old (compared to the young) and negatively enriched in LTDR (compare to the old).

C. Open chromatin intensity (log10 FPKM, ATAC-seq data) of the peaks (p-value< 10^{-5} , merged of all replicates, check the methods) ± 5kb of TSS of the Stat1 target genes with the Stat1 binding motif in liver. P-value is calculated with paired t-test, comparing old with young and LTDR with old.

D and E: GSEA analysis of the Irf3 target genes expression in young versus old (D) and old versus LTDR (E) comparisons (similar to A and B) in liver.

F. Open chromatin intensity of Irf3 target genes with the Irf3 binding motif in liver (similar to C).

G and H: GSEA analysis of the Irf7 target genes expression in young versus old (D) and old versus LTDR (E) comparisons (similar to A and B) in liver.

I. Open chromatin intensity of Irf7 target genes with the Irf7 binding motif in liver (similar to I).

J. Heatmap showing the expression of the top 60 Stat1 target genes (positively regulated by Stat1) which are upregulated in old compared to the young and rescued by LTDR in kidney.